Research article

Effectiveness of soil erosion barriers to reduce sediment connectivity at small basin scale in a fire-affected forest

Manuel López-Vicente [a,*], Henk Kramer [b], Saskia Keesstra [a]

[a] *Team Soil, Water and Land Use, Wageningen Environmental Research, Droevendaalsesteeg 3, Wageningen, 6708RC, Netherlands*
[b] *Team Earth Informatics, Wageningen Environmental Research, Droevendaalsesteeg 3, Wageningen, 6708RC, Netherlands*

ARTICLE INFO

ABSTRACT

Forest fires and post-fire management practices (PFMP) cause changes in the hydrological response of a hillslope. This study evaluates the effect of log erosion barriers (LB) and Easy-Barriers® (EB) on the spatial patterns and values of structural sediment connectivity (SC) in a Mediterranean mountainous pine forest affected by an arson fire in August 2017. A drone flight was done in July 2019 (23 months after the fire and 11 months after the PFMP) to obtain a high-resolution orthomosaic and DEM (at 0.05 m). Two contrasted areas, with and without PFMP, were selected along the same hillslope and 26 small basins were identified: 16 in the treated area (mean area, slope and vegetation recovery of 916 m^2, 60% and 25%; with 94 LB and 39 EB) and 10 in the untreated area (1952 m^2, 75% and 20%). The aggregated index of sediment connectivity (AIC) was chosen to compute SC in three temporal scenarios: Before and just after the fire and when all PFMP were implemented including the incipient vegetation recovery. Output normalization allowed the comparison of the non-nested basins among them. After accounting the intrinsic differences among the basins and areas, and the temporal changes of SC between the three scenarios, the contribution of the barriers was estimated in 27% from the total decrease of SC in the treated area (−8.5%). The remaining 73% was explained by the vegetation recovery. The effectiveness of the LB (11.3% on average) and EB (13.4%) did not diminish with increasing slope gradients. These percentages become relevant considering the small area affected by the LB (2.8%) and EB (1.3%). Independent metrics (convergence index, flow width, flat areas and LS factor) also reported clear differences between the two areas –higher soil erosive intensity in the untreated area– and in accordance with the AIC results.

1. Introduction

Forest fires cause a significant change in the magnitude of the hydrological response of the soil in terms of runoff, soil erosion and sediment and burnt residues transport. In some areas, episodic post-fire erosion that occurs just after a fire can reach very high rates that overcome millennial scale erosion for both channels and hillslopes (Ellett et al., 2019). On steep slopes, fires increase the likelihood of debris flows, inducing geomorphic changes (Tang et al., 2019). In Mediterranean landscapes, where afforestation has been intense during the 20th and 21st centuries –anthropic reforestation for the control of watersheds and natural reforestation for socioeconomic causes (Shakesby, 2011)–, fires negatively affect the provision of ecosystem services such as soil erosion protection, flood mitigation and water quality regulation (Nunes et al., 2018). Ash-loaded post-fire runoff affects water and microbial (higher presence and persistence of pathogens) quality due to the

increased concentration of chemical contaminants (Valenca et al., 2020). Even though the fluxes of dissolved and particulate radionuclides wash-off increased at wildfire-affected forests such as in the Chernobyl Exclusion Zone (Igarashi et al., 2020), the positive aspect, however, is that most erosion and deposition changes happen throughout all catchment compartments in the first one or two years after burning, depending on the intensity of the runoff events (Badía et al., 2015). For two to four years, net sediment accumulation occurs more frequent in the valley bottom (Cerdà, 1998; van Eck et al., 2016; Brogan et al., 2019). It is important to note that prescribed fires, which are used to restore optimum vegetation distribution and to reduce the potential impact of wildfires, do not have a negative impact on runoff and erosion responses (Nouwakpo et al., 2020).

Whilst low-severity fires pose limited threats to the environment or people downstream, high-severity fires cause serious damages that require special efforts like urgent soil stabilization to avoid problems

* Corresponding author.
E-mail addresses: mlopezvicente@gmail.com (M. López-Vicente), henk.kramer@wur.nl (H. Kramer), saskia.keesstra@wur.nl (S. Keesstra).

afterwards (De Luis et al., 2003). Post-fire management practices (PFMP) seek to minimize runoff velocity, soil erosion, seed removal and particulate transport, and with that, decrease sediment connectivity (SC). The term 'sediment connectivity' refers to the water-mediated transfer of soil and sediment particles along the landscape features, and can be explained as the connection degree between the sediment sources at any part of the catchment, and the sites where either temporal/permanent sedimentation take place (disconnectivity) or effective sediment yield predominates (highest connectivity) through the channel network (Hooke, 2003). Post-fire logging is one of the first tasks that authorities promote. However, harvesting dead trees and opening new skid trails can intensify soil erosion due to soil compaction (Prats et al., 2019) and concentrated overland flow that increase the overall SC at catchment scale (Martínez-Murillo and López-Vicente, 2018). Other PFMP effectively stabilize hillslopes, such as afforestation, erosion barriers and soil cover; and reduce sediment transport in the channels, such as dry-stone walls in gullies and check-dams in the main streams (Merino et al., 2019). Log barriers and contour-felled log debris are two common techniques to minimize soil and residues delivery in hillslopes (Badía et al., 2015). These barriers are built with dead trees, favouring the decomposition and incorporation of processed material into the soil and improving physico-chemical and biological soil parameters (Gómez-Sánchez et al., 2019). Recently, an innovative, biodegradable and low-cost solution called Easy-Barrier® was tested in a Mediterranean steep wildfire-affected terrain, resulting in a decrease in the peak flow, a delay in the runoff time at the outlet and a sediment trapping rate of ca. 42.7% (Albert-Belda et al., 2019). Another environmentally friendly alternative is the use of agricultural straw mulch, wood mulch and fibre webs that reduce runoff coefficient and velocity, sediment concentration and flux rate closely to the unburned conditions (Lucas-Borja et al., 2018; Robichaud et al., 2020). However, the life span of the erosion barriers is short and after few years most post-fire works are filled with sediments or collapse (Aristeidis and Vasiliki, 2015). Within the main channels, construction of check-dams is a common emergency practice to avoid flood damage downstream that favour accumulation of fine sediments, organic matter and nutrients, resulting in the development of new vegetated areas (González-Romero et al., 2019). Each PFMP has a different range of effectiveness and distinct spatial and temporal scales of influence on SC. Therefore, the accurate assessment of these hydrological responses is a non-solved research need.

Models and indices are useful tools to map and analyse the changes in runoff and soil erosion/delivery in fire affected areas. For instance, Vieira et al. (2014) used the revised Morgan-Morgan-Finney model to estimate soil losses for burned areas in humid Mediterranean pine and eucalypt forests in north-central Portugal. Also in Portugal, van Eck et al. (2016) used LISEM to simulate rainfall-runoff response, under soil water repellent conditions and different stages of vegetation recovery. The effect of PFMP on the hydrological response of burnt and restored areas can be also evaluated with the assistance of numerical approaches. Indices are simpler –less time-consuming and input-demanding– approaches than models for evaluating a specific process of the soil erosion dynamic. In south-eastern Spain, Martínez-Murillo and López-Vicente (2018) used an index of SC (IC-Borselli) to assess the effect of a fire, different post-fire practices (salvage logging, skid trails and check dams) and vegetation recovery scenarios on the sediment delivery dynamic in headwater sub-catchments. More recently, López-Vicente et al. (2020) evaluated the performance of four indices of SC to compute forest fire and PFMP effects on sediment connectivity in sub-catchments located in a mountainous Mediterranean landscape. However, the impact of PFMP on the spatial patterns and temporal changes of SC at small basin scale (lower than 5000 m^2) remains poorly understood, especially in steep (gradient > 45%) forest slopes, and this study aims to fill this gap.

Remote sensing technologies allow obtaining accurate maps of fire severity, vegetation recovery, topography and other landscape parameters. At large spatial scale, satellite images (e.g. from Landsat, SPOT and Sentinel-2) are useful to calculate the Normalized Burn Ratio (NBR) and Normalized Difference Vegetation Index (NDVI) and multi-temporal indices, such as the difference NBR (dNBR) and difference NDVI (dNDVI), and when this information is combined with models, it is possible to predict how the repeated (historical) fires have impacted vegetation recovery and erosional processes (Fox et al., 2008; Chasmer et al., 2017; Efthimiou et al., 2020). However, low-resolution optical imagery excludes burn losses in transition zones, is not able to distinguish differences in vegetation recovery regarding vegetation height and cannot be used to evaluate small scale erosion features, such as rills and temporal depositional areas. Airborne sensors, such as laser scanners, provide data to quantify erosion and deposition at large scale, and thus, are of interest to evaluate post-fire geomorphic changes over time (Brogan et al., 2019). Unmanned aerial vehicles (UAV), commonly known as drones, have revolutionized the way vegetation (growth and cover) and topographic (digital elevation model – DEM) parameters are measured at low economic and time investments, and at the same time, at high spatial resolution and accuracy (López-Vicente and Álvarez, 2018; Anders et al., 2020). Hua and Shao (2017) reviewed different methods, based on satellite- and drone-mounted sensors, to implement infrared remote sensing applications in forest fire monitoring, highlighting the importance of developing accurate forest masks. The use of UAV imagery enables the assessment of forest canopy fuels and structure by analysing Structure-from-Motion point clouds by using multi-spectral images (Shin et al., 2018). To our knowledge, evaluation of the efficiency of PFMP on minimizing sediment delivery with drone-derived imagery has not been done before, and this study provides a solid basis for further research.

This study aims to evaluate the effectiveness of two types of soil erosion barriers –natural and man-made– to reduce SC at small basin scale in a wildfire affected forest on a steep slope. To achieve this goal, 26 small basins were selected in two contrasted areas, with and without PFMP, along the same hillslope and SC was estimated with the aggregated index of SC (AIC) before and just after the fire and when all PFMP were implemented. Drone imagery allows characterizing ground parameters (e.g. DEM, vegetation patterns) at very high spatial resolution (0.05 m). Independent topographic metrics and spatiotemporal statistical analysis of computed SC was used to quantify the actual role played by the soil conservation measures. The results of this study improve the understanding of the processes of SC in treated and untreated fire affected areas at fine spatial resolution using hydrological basin as research unit. Moreover, results analysis will be of interest for restoration companies and policy makers for better planning PFMP and other forest restoration activities.

2. Materials and methods

2.1. Fire characteristics and post-fire management practices

An arson fire affected the pine forest (*Pinus nigra sub. Salzmannii*; indigenous subspecies) located in the municipality of Segura de la Sierra (Jaen province, Andalusia, south-eastern Spain) between the Trujala River and El Yelmo Mount (1809 m a.s.l.) (Fig. 1a). It started at two different locations (the third one did not burn) on August 3, 2017, expanded rapidly, but was controlled one day later (950 firefighters, 34 aircrafts and 31 terrestrial vehicles) and it was completely extinguished after 25 days. A total of 686.7 ha were burnt, and 270 people were evacuated (González, 2018). According to the effects on tree canopy (see Keeley, 2009 for the use of fire-related terms), fire severity was moderate to high, as all understory vegetation and pine needles burned down, but most burnt trunks and part of the branches remained. The same fire severity was observed in the whole study area. This forest is located in the heart of the 'Sierras de Cazorla, Segura y Las Villas' Nature Park that represents the typical Mediterranean mid-mountain relief with towering rock walls and deep valleys mix with autochthonous pine forests. Therefore, this arson fire caused a serious environmental
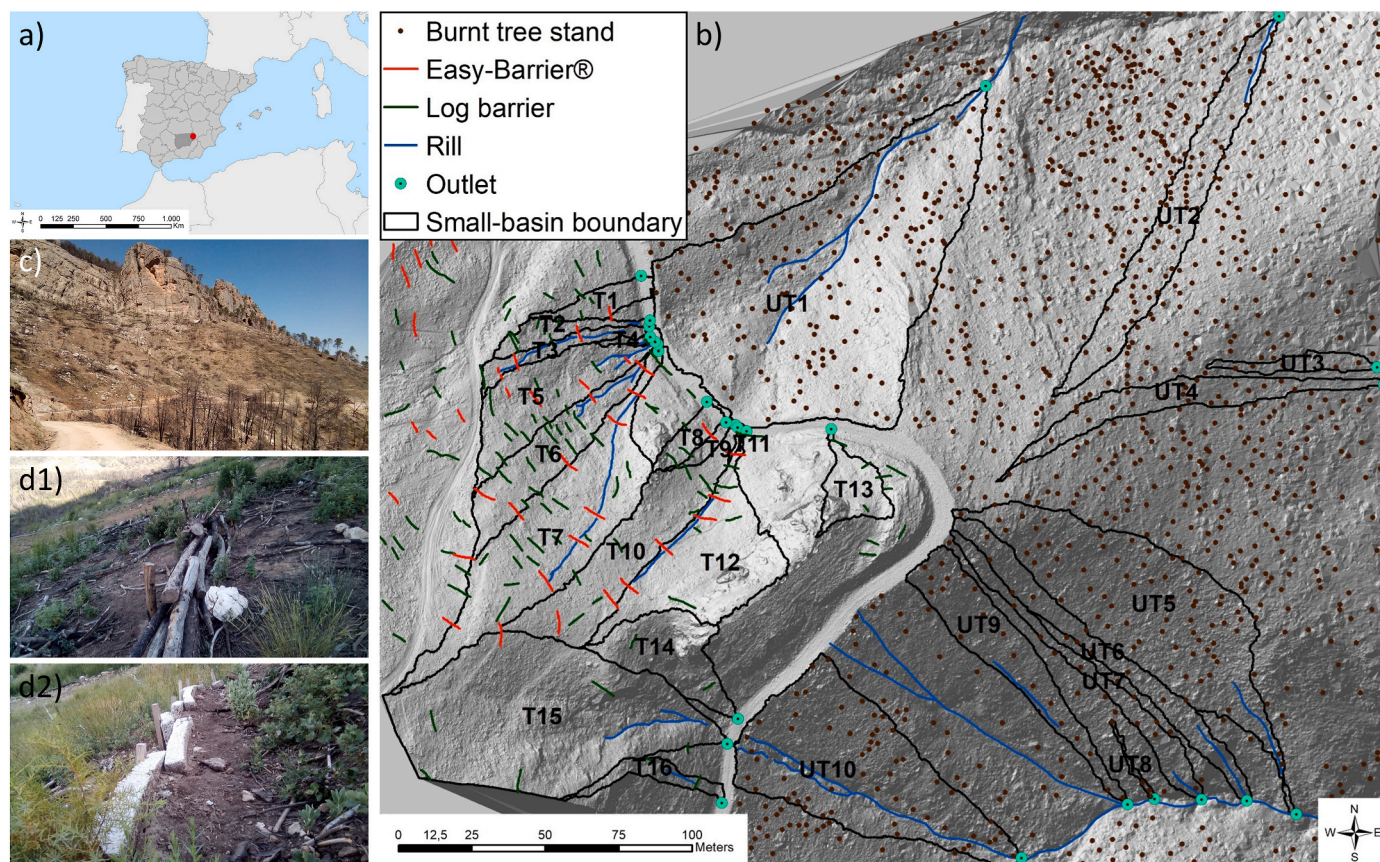
Fig. 1. Location of the study area in south-eastern Spain (Jaen province) (a). Map showing the boundary of the sixteen treated (T; upslope the forest road) and ten untreated (UT; downslope the forest road) small basins with location of the two types of soil erosion barriers and burnt tree stands (b). Pictures of the treated and untreated areas in July 2018 (c), and of the log barriers (d1) and Easy-Barriers® (d2) in June 2019.

damage. Climate in the Nature Park is humid Mediterranean, with an annual rainfall depth between 800 and 900 mm near Segura de la Sierra, distributed between the autumn, winter and spring months, whereas summer is very dry with occasional thunderstorms (data source: 'Diputación Provincial de Jaén'). Daily temperature can be below zero during the winter and hot during the summer.

After the fire, the regional government allocated an emergency action package of 150,000 € and fieldwork started the 25th September. These actions focused on burnt tree removal in some areas and installation of security signals (Velasco, 2018). In spring 2018, the Spanish Ministry of Agriculture and Environment financed measures of hydrological and ash delivery control with a total budget of 250,000 €. During 2019, actions continued at province level (total costs: 800,000 €), both in the burnt and un-burnt forest, including tree thinning and new skid trails (EuropaPress, 2018).

In this study, we focused on a small part of the burnt area where different actions were done related to the (non-)application of PFMP. Namely, we selected a steep hillslope intersected by a forest road (38° 16′ 11.75″ N; 2° 39′ 10.95″ W; see 'FIRE-Jaén-AIC.kmz' file in Supplementary material). No action was done after the fire downslope the road whereas the upslope area was subject to a complete set of PFMP (Fig. 1b and c). These practices included: I) burnt tree removal, II) installation of log erosion barriers (LB hereafter), III) placement of Easy-Barriers® (EB hereafter) and IV) opening of a new skid trail (Fig. 1d). The first, second and fourth measures were done by the regional and national authorities whereas the EB were installed by the staff of the company 'Agroforestal Monte Vivo S.L.' (Jaen, Spain) between 20th July and August 1, 2018. The LB consist of felling burned trees and laying them on the ground along the slope contour (Moreira et al., 2012). Each log was anchored in place, and gaps between the log and soil surface were filled with soil to

create a storage basin on the upslope side of the log where the overland flow is trapped (Fig. 1d1). Each EB consisted of several blocks placed in a zipper arrangement (Fig. 1d2). The number of blocks at each EB was not fixed and was as much as necessary depending on the local characteristics where they were placed. Each block is 80 × 20 × 7 cm in length, height and thickness, respectively. Blocks were not buried and stood on the ground. Wood sticks were driven into the ground to fix the blocks in their place. Blocks are composed by a registered mix of materials, mainly cellulose (from residues that cannot be recycled), diatomites and ashes from burned biomass (more technical details in Albert-Belda et al., 2019). The mean density of the LB and EB per hectare was 64 LB/ha and 27 EB/ha with a mean length of 2 m/LB and 8 m/EB, so equals 340 m of barriers/ha (Table 1). The two types of barriers were placed following the contour lines and according to expert criteria and topographic conditions. Soil was not altered during the installation of LB and EB. The soil in the study area is classified as Cambisol with a significant content of coarse fragments, ca. 25% per volume (source: https://soilgrids.org/). Soil bulk density ranges between 1.1 (topsoil) and 1.5 (at 50-cm depth) g cm^{-3}; and soil texture is loam. The soil organic carbon content ranges between 7% (topsoil) and 0.9% (at 50-cm depth). We did not observe significant changes in the soil type along the selected hillslope.

2.2. Drone flight and images processing

The drone images were taken on June 24, 2019 using a 'DJI – Phantom 4′ drone (technical specifications can be found in the website of the manufacturer). A total of 221 images were taken covering an area of 108,592 m^2 (3D-view). The generated orthomosaic had a spatial resolution of 0.0328 m. Before generating the Structure-from-Motion (SfM) photogrammetry-derived DEM, point clouds representing

Table 1
Main characteristics of the small basins in the Post-fire scenario.

Zone	Basin	Area	Slope gradient	RT	Rock outcrop	Log barrier	Easy-Barrier®	Barrier length	Burnt tree	Burnt tree density	Vegetation recovery[a]
Type	ID	(m^2)	(%)	[0–1]	(m^2)	(n)	(n)	(m)	(n)	(n/ha)	(m^2; %[b])
Treated	T-1	281.6	51 ± 28	0.892	1.7	4	1	10.0	ND	ND	60.5; 21.6%
	T-2	265.2	55 ± 26	0.877	7.2	6	1	19.3	ND	ND	53.9; 20.9%
	T-3	284.9	52 ± 25	0.884	4.1	2	3	15.7	ND	ND	73.9; 26.3%
	T-4	38.9	58 ± 25	0.882	0.6	1	0	1.3	ND	ND	10.6; 27.6%
	T-5	1152.0	56 ± 25	0.870	6.7	12	5	64.9	ND	ND	277.4; 24.2%
	T-6	992.5	57 ± 24	0.867	0.9	14	5	75.3	ND	ND	260.7; 26.3%
	T-7	2463.4	53 ± 24	0.864	98.3	18	10	124.6	ND	ND	613.5; 25.9%
	T-8	225.8	66 ± 29	0.896	51.8	3	1	16.8	ND	ND	40.0; 23.0%
	T-9	86.2	65 ± 26	0.889	13.8	3	1	4.4	ND	ND	19.5; 27.0%
	T-10	1507.0	53 ± 24	0.874	33.4	9	5	61.6	ND	ND	360.0; 24.4%
	T-11	16.7	56 ± 27	0.892	0.0	1	1	2.6	ND	ND	3.4; 20.6%
	T-12	1626.3	59 ± 26	0.884	430.8	8	5	49.3	ND	ND	337.3; 28.2%
	T-13	438.1	56 ± 28	0.897	118.0	4	0	8.4	ND	ND	108.2; 33.8%
	T-14	878.6	71 ± 28	0.891	146.8	2	0	8.5	ND	ND	172.6; 23.6%
	T-15	4147.3	65 ± 27	0.865	14.1	5	1	28.9	ND	ND	950.7; 23.0%
	T-16	251.9	80 ± 23	0.907	0.0	2	0	6.0	ND	ND	54.5; 21.7%
	MEAN	*916*	*59.6*	*0.883*	*58.0*	*5.9*	*2.4*	*31.1*	*ND*	*ND*	*24.7%*
Untreated	UT-1	7243.4	66 ± 25	0.880	543.5	0	0	0	157	217	1442.7; 21.5%
	UT-2	1595.2	74 ± 23	0.905	1.4	0	0	0	55	345	259.1; 16.3%
	UT-3	247.1	70 ± 19	0.934	0.0	0	0	0	6	243	18.2; 07.4%
	UT-4	910.8	70 ± 20	0.913	5.6	0	0	0	23	253	200.6; 22.2%
	UT-5	3480.3	73 ± 24	0.889	22.6	0	0	0	65	187	673.8; 19.5%
	UT-6	986.3	76 ± 24	0.897	5.7	0	0	0	9	91	193.7; 19.8%
	UT-7	643.2	78 ± 23	0.904	2.3	0	0	0	7	109	119.9; 18.7%
	UT-8	45.3	81 ± 25	0.919	0.0	0	0	0	4	883	7.2; 15.8%
	UT-9	1228.5	81 ± 21	0.893	4.4	0	0	0	19	155	199.0; 16.3%
	UT-10	3140.0	78 ± 23	0.889	20.4	0	0	0	55	175	668.9; 21.4%
	MEAN	*1952*	*74.7*	*0.902*	*60.6*	*0*	*0*	*0*	*40*	*205*	*20.0%*

RT: Residual topography (see Eq. (2)).

[a] New shrubs and herbs after the fire.

[b] Percentage from the total area of each small basin after excluding the area occupy by the outcrops. ND: No data.

vegetation (e.g., trunks and branches) and infrastructures had to be removed and the different filtering techniques have various degrees of success in different use cases (Anders et al., 2019). In this study, we used the following four-step process: I) photos processing and generation of the point cloud with *Pix4Dmapper* (Pix4D S.A. Prilly, Switzerland); II) ground point classification with *LAStools* (rapidlasso GmbH. Gilching, Germany); III) manual correction of ground point classification with *ArcGIS Pro* (Esri. Redlands, USA) owing to the presence of big steep outcrops that were not classified as ground in step II; and IV) DEM generation, at 0.05×0.05 m of cell size, by interpolating the ground points.

The high contrast levels between the colours of the burnt vegetation (dark grey and brown), rock outcrops (light grey), soil (brown), LB (dark brown), EB (white) and new vegetation (green) allowed us to estimate the soil surface area covered by the new vegetation –grown after the fire– using the orthomosaic. The RGB image was converted to palette (PCT) image using the Tool 'conversion' of *QGIS* (a free and open source GIS). This tool classifies pixels into groups of similar colour. After having tried a number of groups and compared the results with field pictures –to guarantee the correct grouping–, we reduced the RGB image to an eight-colour PCT image. Then, the PCT image was simplified to a two-colour image to calculate the number of pixels of the new vegetation.

2.3. Small basins and simulated scenarios

In total, 26 small basins were selected following these criteria: I) representative of the distinct conditions in the treated (T-A; with 16 basins) and untreated (UT-A; with 10 basins) areas; II) non-nested sub-catchments (to avoid autocorrelation); and III) of different sizes in order to better account the effect of the upslope drainage area on the assessment of SC (Fig. 1b). The mean area and slope gradient of the small basins in the T-A and UT-A are 916 and 1952 m^2 and 60% and 75%, respectively (Table 1). The rock outcrops –mainly Cretaceous sandstones and limestones– represent 6% and 3% of the total T-A and UT-A, respectively. In total, 94 log barriers and 39 Easy-Barriers® were installed in the basins of the T-A with a mean barrier length of 31 m per small basin. New vegetation was observed in 24.7% of the pixels in the T-A (ranging between 20.6% and 33.8% in the 16 small basins) and 20.0% in the UT-A (ranging between 7.4% and 22.2% in the 10 small basins). In the UT-A, the density of burnt trees ranged between 91 and 883 burnt trees/ha per small basin with a mean value of 205 burnt trees/ha.

To better assess the actual role played by the soil erosion barriers and compare the T-A and UT-A, we needed to know the differences in SC between the 26 selected small basins before the PFMP were implemented. To achieve this goal, we selected three temporal scenarios to compute SC with AIC (Table 2). The Pre-fire scenario represents the

Table 2
Simulated scenario of sediment connectivity and main forest characteristics and practices.

Selected small basins		Scenario		
Type	Number	Pre-fire (2014)	Fire (August 2017)	Post-fire (July 2019)
Treated	16	Pine forest	Burnt	Tree removal, Skid trail, Log barriers, Easy-Barriers®
Untreated *Inputs with temporal changes*	10	Pine forest - Smooth DEM[a] - Land use: SIOSE2014	Burnt - Smooth DEM[a] - Land use: SIOSE2014 + Fire severity	No measure - Drone-derived DEM - Land use: SIOSE2014 + Fire severity + Vegetation recovery mask + Barriers mask

[a] A modified version of the drone-derived DEM in order to minimize the influence of the erosion barriers on the micro-topography.

physiographic conditions before the fire. In the Fire scenario, SC was estimated just after the fire; and the Post-fire scenario refers to the conditions at the time of the drone flight (23 months after the fire and 11 months after the PFMP).

2.4. Aggregated index of sediment connectivity (AIC)

In this study, we used the Aggregated Index of sediment Connectivity (AIC) proposed by López-Vicente and Ben-Salem (2019). This index is based on the original Borselli's et al. (2008) index (IC), it includes some modifications related to the slope gradient and overland flow accumulation algorithm and it integrates new factors related to the residual topography, rainfall erosivity and soil permeability. The AIC equation allows to assess both structural and functional sediment connectivity at distinct spatial scales, from small fields to medium and large catchments, and under different physiographic and land use conditions, such as croplands (Gogorcena et al., 2019), agro-ecosystems (López-Vicente and Ben-Salem, 2019) and fire-affected areas (López-Vicente et al., 2020). This index is defined in the range of $[-\infty, +\infty]$ and connectivity increases when the index tends to $+\infty$.

The AIC accounts for the role played by the drainage area and flow path characteristics at each pixel. The downslope module (D_{dn}) contemplates the probability that runoff and sediment arrive at a user-defined computation target (e.g., sink, check-dam, outlet, channel or stream system). The upslope module (D_{up}) represents the potential for downward routing of overland flow occurring upslope and also implements a "stream power"-like approach, taking into account the weighting factors and size of the drainage area:

$$AIC_k = \log_{10}\left(\frac{D_{up,k}}{D_{dn,k}}\right) = \log_{10}\left(\frac{\overline{AWC_t} \cdot \sqrt{A_k}}{\sum_{k=i}^{n} \frac{d_i}{AWC_i}}\right) \tag{1}$$

$$AWC_i = R_{ti} \cdot RT_i \cdot C_{ti} \cdot K_{Pi} \cdot S_i \tag{2}$$

where AWC is the aggregated weighting factor at (sub-)catchment scale, A is the upslope drainage area (m²), d_i is the length of the ith cell along the downslope path (m), R_t is the normalized rainfall erosivity factor for the period t (values between 0 and 1), RT is the residual topography factor (normalized values between 0 and 1), C_t is the vegetation (crop and natural vegetation) management factor for the period t (values between 0 and 1), K_P is the soil permeability factor (normalized values between 0 and 1) and S is the slope gradient (m/m). The subscript K indicates that each cell 'i' of the (sub-)catchment has its own value of sediment connectivity.

The weighting component AWC (called 'W' in the Borselli's et al. (2008) approach) was introduced to calculate the impedance to runoff and sediment fluxes due to properties of the local land use and soil surface. The K_P factor allows to account the spatially distributed influence of the soil physical properties because significant spatial changes appear in the values of soil water content along the hillslope (López-Vicente et al., 2009), and these changes have a clear effect on runoff generation at hillslope scale (Zhang et al., 2019). The C-factor of the RUSLE (Renard et al., 1997) and RUSLE2 (USDA, 2008) soil erosion models reflects the effect of cropping and management practices of the different land uses on the soil erosion rates. The RT factor estimates the role of the microtopography homogeneity/heterogeneity on the impedance of overland flow. In order to minimize the temporal variability between the evaluated scenarios in this study and to focus the analysis on the sole effect of the soil erosion barriers, the rainfall erosivity factor was set to a value of $R_t = 1$ in the three scenarios.

Index setup includes several conditions. In Eq. (2), slope gradient of less than 0.005 must be adjusted to $S_i = 0.005$ and higher than 1 must be set to a maximum value of $S_i = 1$. The weighted flow path length and upslope factors ($\overline{R}$, $\overline{RT}$, $\overline{C}$, $\overline{K_P}$ and $\overline{S}$) were calculated using the D-Infinity

algorithm available in *SAGA* (a free and open source GIS). In this study, the user-defined computation target was the outlet of each small basin and is based on the Flow-Direction map. Those pixels that are considered the target of the SC assessment have a value of Flow-Direction equals to zero. These changes do not affect the general SC Eq. (1) and only affect the computation of the downslope component (D_{dn}). As AIC outputs are dimensionless indicators that depend on the spatial location of the computation target, the AIC values were normalized in order to have comparable values of SC (AIC_N) between the small basins. We proposed the following expression:

$$AIC_N = AIC_i \times \log_{10}(10 + FlowLength_{outlet}) \tag{3}$$

Value normalization was done for each small basin independently, in order to use the flow path length (in meters) of each small basin considering the user-defined outlet as the reference point. This means we used the modified flow direction map –generated for the computation target– to estimate the flow length map. The topographic linear slope length factor was selected because it influences noticeably soil erosion on hillslopes (Yair and Raz-Yassif, 2004) and its values depend on the spatial location of the outlet. Equation (3) can be used for any range of values of AIC_i, pixel size and catchment area. This approach tries to solve one of the shortcomings of the IC-family approaches in the comparative study of different catchments among them.

Before computing the index, the small local depressions (artefacts) of the drone-derived DEM were removed using the Planchon and Darboux algorithm (available in *SAGA*) without adding unrepresentative flat surfaces. A minimum gradient of 0.01° was set to ensure flow routing across the filled sinks. Then, the boundary of the upslope drainage area of each small basin was calculated from the location of the outlet upwards using the flow accumulation map. The new skid trail, located in the north-western part of the study area, acted as water divide for the small basins T3, T5 and T7 and it remained outside the selected basins. A smooth DEM was generated and used in the Pre-fire and Fire scenarios in order to minimize the effect of the soil erosion barriers on the micro-topography, and thus, to depict the topographic conditions before the PFMP. The smooth DEM was obtained using the 'Residual Analysis (Grid)' tool (*SAGA* software), with a radius of 3 cells –including the centre cell– that created a 7 × 7 moving average window (0.35 × 0.35 m). The size of this window is slightly larger than the thickness of the LB (ca. 30 cm) and EB (7 cm), and thus, the smooth DEM averaged effectively the micro-topography surrounding the barriers without affecting too much the remaining areas. The weighted flow path length and upslope factors of the Pre-fire and Fire scenarios were calculated using the smooth DEM.

The residual topography factor, RT in Eq. (2), was obtained as the normalized and inverse values of the standard deviation of the slope gradient. A minimum RT value of 0.001 was set to avoid computational errors. The soil permeability factor, K_P in Eq. (9), was obtained using the map of lithostratigraphic units of the Spanish Geological Survey (IGME; at 1:50,000). The lowest value ($K_P = 0.25$) was assigned to the unit with higher permeability (sandstone) and moderate ($K_P = 0.50$) and higher ($K_P = 0.75$) values corresponded to the units with moderate (limestone) and low (mainly clay) permeability, respectively. The rock outcrops were considered as non-permeable ($K_P = 0.99$). The main input maps are presented in the Supplementary Figure 1.

Three C-factor maps were generated, one per scenario (Table 2). In the Pre-fire scenario, we used the available land use and land cover (LULC) map of year 2014 generated by the Spanish National Centre of Geographic Information (IGN; SIOSE system of classification at 1:25,000). Although this map is accurate and includes four different land uses in the study area, we modified it in order to ensure the inclusion of four important land uses: I) the forest road; II) the skid trail; III) the rock outcrops; and IV) the gullies. Each SIOSE land cover polygon is a combination of several land uses, such as "coniferous plantation (65%), bare soil (25%), with presence of pasture (5%) and shrubs (5%)". For each land use, we used the harmonized values proposed by Panagos

et al. (2015) in a review article made for the 28 countries of the European Union. The C-factor map of the Fire scenario was obtained by multiplying the Pre-Fire C-factor map with the weighted map of burn severity (homogeneous moderate-high in the whole study area). For this calculation, we used the weighting values proposed by Larsen and MacDonald (2007), and Yochum and Norman (2015): low burn = 1.10, moderate burn = 2.25 and high burn = 3.75. The C-factor map of the Post-Fire scenario was generated by combining the Fire C-factor map with the masks of vegetation recovery and soil erosion barriers. In the identified pixels with new vegetation, we assigned a C-factor of 0.05985 (averaged between C-factors for scrubland and pasture in Panagos et al., 2015). The erosion barriers mask was made using the orthomosaic and polygons were drawn up-slope (between 0.40 and 0.70 m) and down-slope (between 0.05 and 0.35 m) from each barrier covering the area where the influence of the barrier clearly appears, which means: I) trapping sediments; II) higher vegetation recovery; and III) lack of rills. The effectiveness of log-erosion barriers has been evaluated in different places, under distinct physiographic and forest-type conditions, obtaining distinct, and in some cases non-conclusive, results (e.g. Wohlgemuth et al., 2001; Raftoyannis and Spanos, 2005; Fernández et al., 2011). Therefore, we selected those studies made in pine forest under Mediterranean conditions, that are those comparable to our study site. In the polygons of the erosion barriers mask, we considered a C-factor reduction of 52% and 43% for the LB and EB, respectively, based on the field studies made in eastern Spain by Badía et al. (2015) with LB and by Albert-Belda et al. (2019) with EB. In other Mediterranean fire-affected pine forest, Aristeidis and Vasiliki (2015) found that peak discharge declined by 10.5% and 20.4% in two steep catchments and sediment yield minimized by 11% and 25% due to the effect of hillslope PFMP, including LB; the differences were attributed to more efficient work construction in one of the two catchments. To avoid an overestimation of the effect of the two masks on the assessment of SC, the overlay between the masks of new vegetation and erosion barriers was not allowed. In the Pre-fire, Fire and Post-fire scenarios, the mean *C* factor value in the T-A was 0.0960, 0.1454 (51% higher than before the fire) and 0.1310 (10% lower than after the fire and 36% higher than before the fire); and in the UT-A was 0.1418, 0.2757 (94% higher than before the fire) and 0.2358 (14% lower than after the fire and 66% higher than before the fire).

2.5. Statistical analysis and metrics for evaluation

First, the differences between the small basins of the T-A and UT-A were analysed in the Pre-fire and Fire scenarios. This results analysis gave us the information of the intrinsic differences among the small basins before the PFMP were done. Then, we calculated the distinct magnitude and spatial patterns of SC between the T-A and UT-A in the Post-fire scenario, at small basin and total area scales. Finally, we joint the two datasets to quantify the actual role played by the two types of soil erosion barriers. The statistical analysis of the differences between the two areas and the three scenarios was done by calculating the ANOVA with Tukey test (95% of confidence).

Independent metrics –not included in the index inputs– were used to evaluate the accuracy of the output index in the 26 small basins and between the two treatment areas. Four structural metrics that only depends on the physical structure of the landscape was selected, namely: The convergence index (CI), flow width (FW), flat areas (FA) and LS-factor (LS). The CI, proposed by Köthe et al. (1996), uses the aspect values of neighbouring cells to parameterise flow convergence and subsequently divergence. It is similar to plan curvature, but does not depend on absolute height differences. It calculates the smooth horizontal curvature as a percentage; negative values correspond to convergent and positive to divergent flow conditions. So a value of +100 would represent the peak of a cone, −100 a pit, and 0 a flat surface. The CI is useful in lineament analysis, especially those represented by ridges or channel systems, and also as a valley recognition tool. The FW or

effective contour length orthogonal to the outflow, proposed by Gruber and Peckham (2008), is another important concept in hydrology and for flow-based parameters. The 'Flat detection' tool identified disconnected areas without a direct link with the overland flow pathway and outlet of the small basin. The LS-factor is the topographic component of the RUSLE model of soil erosion (Renard et al., 1997). These metrics were calculated using tools available in *SAGA* and evaluating the soil surface, and thus, avoiding the areas with rock outcrops. The combined analysis of these metrics refines the evaluation of the existing differences between the T-A and UT-A regarding the topographic anisotropy in the different landscape compartments.

3. Results and discussion

3.1. Differences in SC between the small basins in the pre-fire and fire scenarios

In the Pre-fire and Fire scenarios, the estimated maps of SC showed clear differences between the T-A and UT-A (Fig. 2). Before the fire, the average value of SC in the 16 basins of the T-A ($\overline{AIC_N} = -13.2 \pm 3.8$) was 17% lower than the average value of SC in the 10 basins of the UT-A ($\overline{AIC_N} = -11.3 \pm 2.5$) (Table 3). In the Fire scenario, this difference increased up to −20% owing to the distinct increases of SC in the T-A (9% higher SC; $\overline{AIC_N} = -12.0 \pm 3.6$) and UT-A (11% higher SC; $\overline{AIC_N} = -10.0 \pm 2.3$). However, the differences between the mean values of SC of the basins included in the two areas were not significant in the Pre-Fire ($P = 0.283$) and Fire ($P = 0.181$) scenarios. The differences between the estimated SC in the two areas are explained by the different magnitude of the AIC inputs in the T-A and UT-A. In particular, the mean values of all inputs were higher in the UT-A than in the T-A: Slope gradient (21% higher), residual topography (2% higher), C-factor in 2014 (48% higher), C-factor in 2017 (90% higher) and soil permeability factor (101% higher). The influence of these factors on the intensity of sediment delivery and transport have been proved in many studies at different spatial scales and resolutions, and thus, the AIC outputs agree with the observations reported in the available literature. For instance, Tarolli et al. (2019) measured the influence of micro-topography factors, such as roughness, slope and curvature, at high spatial resolution (2 cm), affecting surface runoff and sediment transport. Pena et al. (2020) evaluated different land uses and the effect of their cover-management factors on soil erosion rates, emphasizing the relevance of distinct soil cover protection values on the spatial identification of the main soil erosion affected areas. Nishigaki et al. (2017) observed in mountainous areas that runoff coefficients and sediment concentrations are usually lower at sites with high soil water permeability despite similar rainfall depths in comparable areas with lower permeability.

Regarding the effect of the forest fire, the estimated SC increased in all basins, ranging from +3.5% to +12.6% in the basins of the T-A ($\overline{\Delta SC} = +9.2\%$) and from +8.2% to +13.9% in the basins of the UT-A ($\overline{\Delta SC} = +11.3\%$) (Fig. 3). Despite these clear changes, the differences between the mean values of SC in the Pre-Fire and Fire scenarios were not significant in the T-A ($P = 0.376$) and UT-A ($P = 0.117$). These results were in accordance with the field measurements, using plots and collectors, of higher values of soil erosion and sediment transport obtained in fire-affected forests in countries/regions under Mediterranean climate, such as Spain (Martínez-Murillo et al., 2016, Martínez-Murillo et al., 2016), Greece (Blake et al., 2010), Israel (Inbar et al., 1998) and California (De Koff et al., 2006). Mediterranean pine species and soil surface conditions in the mountainous areas –soil water repellency is a widespread property of fire-affected pine forest soils in south-eastern Spain (Mataix-Solera et al., 2011)– favour the rapid increase of runoff yield and sediment concentration after the fire (Cerdà et al., 2017). However, in some environments in northern countries, such as the boreal forests of Canada, the thick soil organic layers can remain above the mineral soil even after many high-intensity wildfires, and thus, soil erosion increases
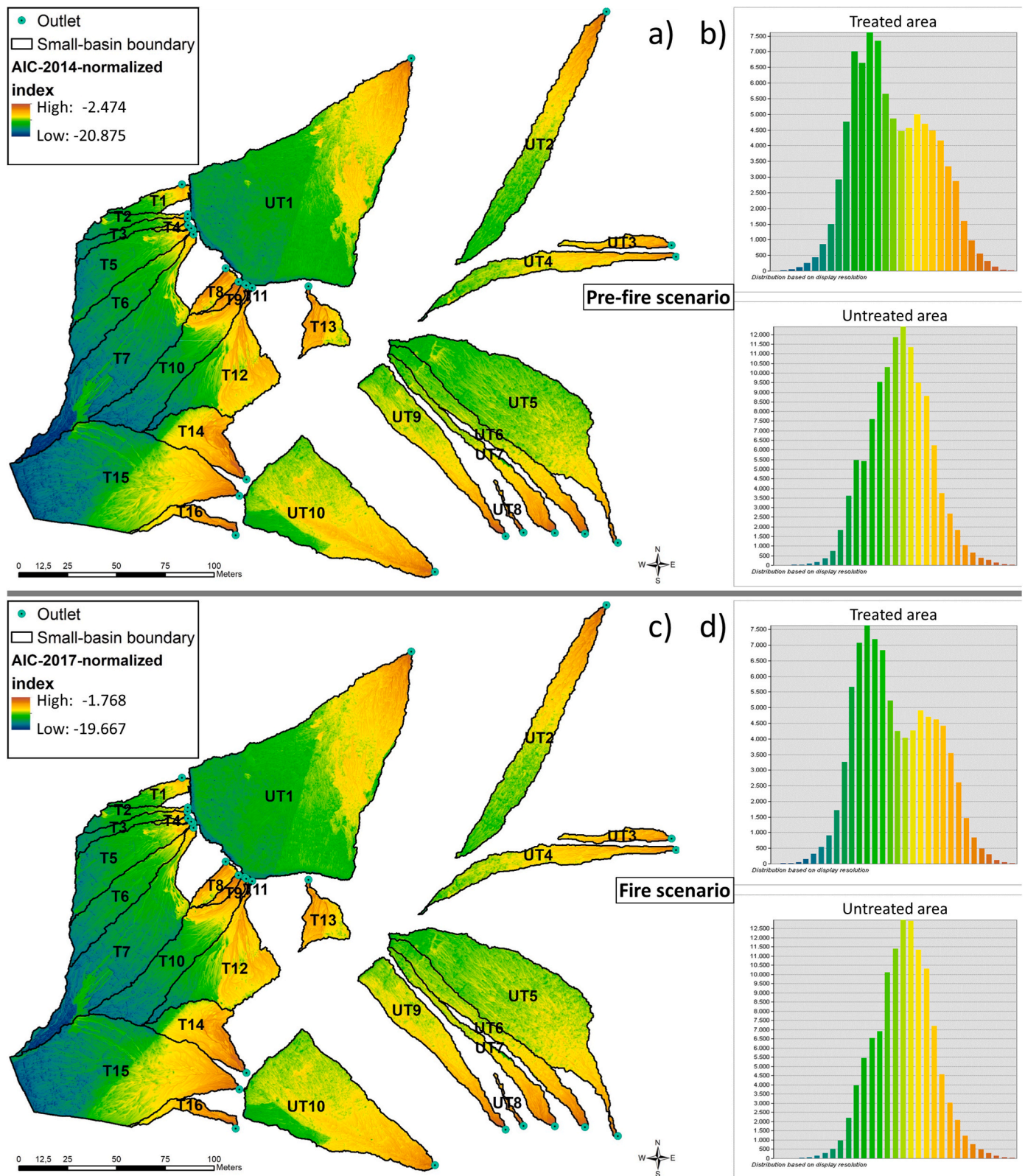
Fig. 2. Maps of estimated sediment connectivity (AIC_N) in the Pre-fire (a) and Fire (c) scenarios, and frequency distribution of the values in the treated and untreated small basins (b, d).

in post-wildfires years is almost negligible (Martin et al., 2011). Therefore, the temporal changes in the spatial values of SC estimated with the AIC before and after the fire in the T-A and UT-A can be considered as realistic and trustworthy.

For a better understanding of the processes and the spatial patterns of SC, the histograms of the generated maps were calculated at each area (Fig. 2b,d). In the Pre-Fire scenario, a bimodal distribution appeared in the T-A whereas a unimodal distribution was characteristic of the UT-A.

Table 3
Estimated values of SC in the small basins in the Pre-fire, Fire and Post-fire scenarios.

Zone	Basin	Pre-fire	Fire		Post-fire		
Type	ID	mean ± sd	mean ± sd	Δ*	mean ± sd	Δ*	Δ**
Treated	T-1	−11.3 ± 2.3	−10.4 ± 2.0	+7.8%	−11.0 ± 2.0	+2.9%	−5.4%
	T-2	−13.8 ± 2.1	−12.7 ± 1.9	+8.3%	−13.3 ± 2.0	+4.1%	−4.6%
	T-3	−14.1 ± 2.6	−12.8 ± 2.4	+8.8%	−13.4 ± 2.4	+4.6%	−4.5%
	T-4	−9.7 ± 1.5	−8.9 ± 1.3	+8.8%	−9.5 ± 1.3	+2.5%	−6.9%
	T-5	−14.5 ± 2.2	−13.2 ± 2.0	+8.9%	−13.9 ± 2.1	+4.2%	−5.2%
	T-6	−14.9 ± 2.1	−13.6 ± 2.0	+8.7%	−14.5 ± 2.0	+2.6%	−6.7%
	T-7	−15.8 ± 2.6	−14.5 ± 2.4	+8.3%	−15.6 ± 2.3	+1.8%	−7.0%
	T-8	−7.5 ± 1.7	−7.2 ± 1.6	+3.5%	−8.1 ± 1.5	−9.1%	−13.2%
	T-9	−6.4 ± 1.3	−5.8 ± 1.2	+9.3%	−7.3 ± 1.3	−12.8%	−24.4%
	T-10	−14.1 ± 3.5	−12.9 ± 3.2	+8.8%	−13.8 ± 3.0	+2.2%	−7.2%
	T-11	−6.7 ± 1.1	−5.9 ± 1.0	+11.6%	−7.2 ± 1.0	−7.8%	−21.9%
	T-12	−10.8 ± 3.1	−9.8 ± 2.8	+9.4%	−11.2 ± 2.5	−3.0%	−13.7%
	T-13	−8.0 ± 1.7	−7.2 ± 1.5	+10.9%	−8.6 ± 1.5	−7.6%	−20.7%
	T-14	−8.9 ± 2.8	−7.9 ± 2.6	+11.5%	−8.9 ± 2.4	+0.4%	−12.6%
	T-15	−13.9 ± 3.7	−12.5 ± 3.6	+9.9%	−13.6 ± 3.4	+2.1%	−8.6%
	T-16	−7.7 ± 1.9	−6.8 ± 1.7	+12.6%	−7.9 ± 1.7	−1.6%	−16.2%
	All	*−13.2 ± 3.8*	*−12.0 ± 3.6*	*+9.2%*	*−13.0 ± 3.4*	*+1.5%*	*−8.5%*
Untreated	UT-1	−12.7 ± 2.7	−11.3 ± 2.5	10.8%	−11.9 ± 2.6	+6.3%	−5.0%
	UT-2	−10.5 ± 2.3	−9.1 ± 2.1	13.1%	−9.4 ± 2.3	+10.2%	−3.3%
	UT-3	−8.0 ± 1.3	−6.9 ± 1.2	13.9%	−7.0 ± 1.3	+12.9%	−1.3%
	UT-4	−10.1 ± 1.8	−8.7 ± 1.6	13.2%	−9.1 ± 1.8	+9.3%	−4.5%
	UT-5	−11.5 ± 1.4	−10.1 ± 1.3	12.4%	−10.6 ± 1.3	+7.7%	−5.3%
	UT-6	−10.3 ± 2.2	−9.0 ± 2.0	12.9%	−9.4 ± 2.1	+8.5%	−5.0%
	UT-7	−9.4 ± 2.3	−8.2 ± 2.2	12.1%	−8.6 ± 2.2	+8.1%	−4.6%
	UT-8	−6.5 ± 1.8	−5.6 ± 1.6	13.9%	−6.0 ± 1.5	+8.2%	−6.6%
	UT-9	−10.1 ± 1.8	−8.8 ± 1.6	12.9%	−9.2 ± 1.7	+8.1%	−5.5%
	UT-10	−10.1 ± 2.0	−9.3 ± 1.7	8.2%	−9.9 ± 1.7	+2.0%	−6.7%
	All	*−11.3 ± 2.5*	*−10.0 ± 2.3*	*+11.3%*	*−10.5 ± 2.4*	*+6.7%*	*−5.2%*
T *vs.* UT	*Areas*	−17.4%	−20.1%	−18.4%	−23.9%	−77.7%	+64.5%
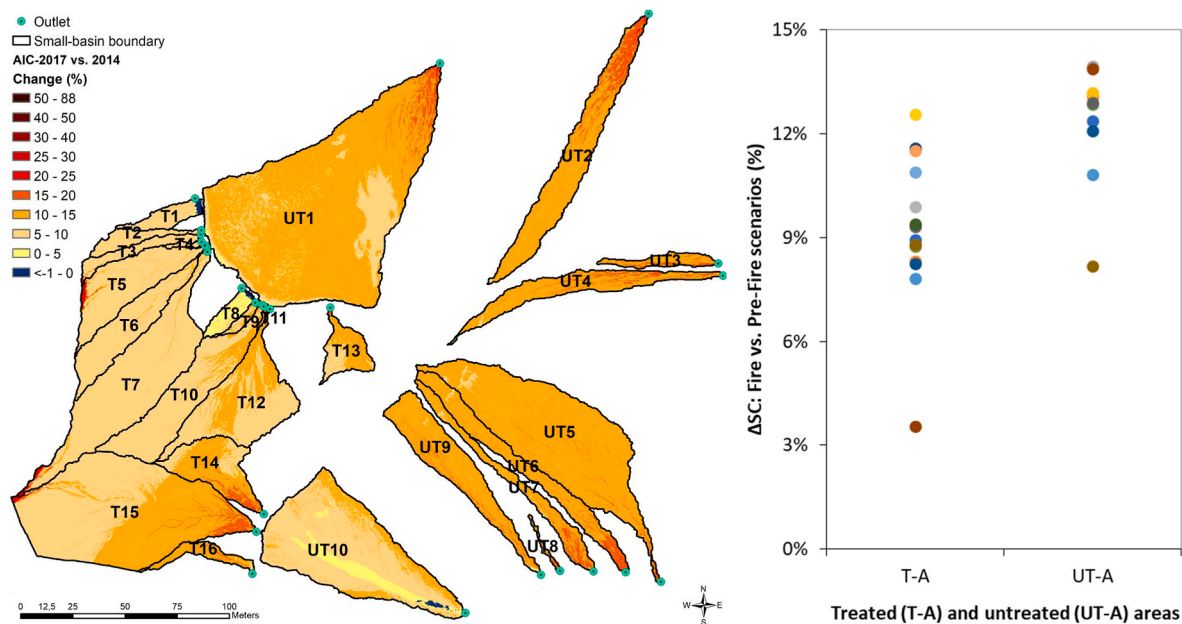
Fig. 3. Changes in sediment connectivity between the Fire and Pre-fire scenarios: (a) map, and (b) at basin scale.

Table 4
Values of linear correlation coefficients (Pearson's r) between the mean values of estimated sediment connectivity ($\overline{AIC_N}$) in the Pre-Fire and Fire scenarios and the index inputs.

Scenario	Slope	Residual topography	Rocks	C-2014	C-2017	C-2019	Permeability
Index	m/m	[0–1]	m²	[0–1]	[0–1]	[0–1]	[0–1]
$\overline{AIC_N}$ Pre-Fire	0.516	0.753	−0.118	0.590	–	–	0.476
$\overline{AIC_N}$ Fire	0.555	0.779	−0.117	–	0.713	–	0.519
$\overline{AIC_N}$ Post-Fire	0.610	0.839	−0.151	–	–	0.673	0.573

This pattern remained in the Fire scenario, but with a more irregular distribution of the SC values: The bimodal distribution in the T-A was more marked and the normal-type distribution in the UT-A was less symmetric. Regarding the relative influence of the different inputs, correlations were estimated between the mean values of each input and the corresponding $\overline{AIC_N}$ per basin and scenario (Table 4). The residual topography and land use and cover management factors, RT and C in Eq. (2), showed the highest linear correlations (Person's r) with $\overline{AIC_N}$, with r values between 0.75 and 0.84 for RT and between 0.59 and 0.71 for C. The slope gradient and soil permeability factors, S and K_P in Eq. (2), correlated less, with r values between 0.52 and 0.61 for S and between 0.48 and 0.57 for K_P. These influences explain the high values of SC in T-4, T-8, T-9, T-11, T-13, T-14, T-16 and UT-3, UT-7 and UT-8, where the index inputs have their highest values. However, no threshold value has been found in the inputs that could explain an important change in the estimated values of SC (Sup. Fig. 2). This results analysis agree with the findings obtained in comparable Mediterranean forests where the relative role played by the main physiographic factors has been estimated. For instance, Badía et al. (2008) found in field experiments conducted in northern Spain that soil cover and soil surface roughness significantly influence the hydrological and erosive response of burnt soils. Nasta et al. (2017) reported clear differences in water budget and sediment transport owing to land use and land cover changes in mountainous areas in southern Italy. Regarding soil physicochemical properties, Inbar et al. (2014) observed in a fire-affected forest in northern Israel that soil permeability changed due to the fire –altered soil water repellency (SWR)–, and clearly affected the runoff and soil loss amounts. As SWR is a key factor in post-fire runoff and soil erosion, and its persistence and intensity depends on fire intensity, vegetation type and species, soil depth and acidity, etc.; all of them creating complex wetting and water repellent three-dimensional soil patches (Zavala et al., 2009), we consider that further versions of the AIC should include a specific sub-factor related to SWR, probably associated with the K_P factor.

3.2. Effectiveness of the soil erosion barriers to reduce SC after the fire

In the Post-fire scenario and compared to the Fire scenario, the mean value of SC decreased 8.5% in the T-A ($\overline{AIC_N} = -13.0 \pm 3.4$) and 5.2% in the UT-A ($\overline{AIC_N} = -10.5 \pm 2.4$), and thus, the loss of SC was, on average, 64% higher in the T-A than in the UT-A (Table 3). Compared with the conditions before the fire, the current mean value of SC remains 1.5% higher in the T-A and 6.7% higher in the UT-A. Therefore, the average magnitude of SC in the T-A is quite similar to the prevalent conditions before the fire, whereas the magnitude of SC in the UT-A is still higher. These results can be explained by the combined effect of the vegetation recovery –different in the T-A and UT-A– and by the presence of the soil erosion barriers. The higher vegetation recovery in the T-A compared with the UT-A (24% larger surface) agrees with the field observations made by other authors in restored forests after fires. For instance, Spanos et al. (2010) assessed in *Pinus halepensis* forests in northern Greece that 2 years after treatment application (seeding, logging and building of log barriers), 70–80% of the ground in all sites was covered with vegetation. Lee et al. (2014) observed 4 years after a large forest fire in South Korea that the recovery of native plant species was more efficient in areas under rehabilitation treatments (ground seeding, hydroseeding, tree planting, sodding, vegetation sacks, log erosion barriers) compared with the results in the untreated site, being the log erosion barrier treatment critically effective in reducing the sediment yield because it provided storage spaces. The accurate assessment of vegetation recovery plays a key role in the estimation of SC after the fire. Therefore, further research with UAV should consider the use of multispectral imaging sensors that could improve the precise quantification of the ground covered by and size/shape of the new vegetation (Guo et al., 2019).

The effect of the barriers became more relevant in the steepest areas, as we found a positive logarithmic correlation ($R^2 = 0.2214$) between

the reduction of SC ($\Delta\overline{AIC_N}_{(\text{Post-Fire vs. Fire})}$) and the increment of slope gradient. The average decrease of SC was of 9.4%, 15.4% and 14.4% in the basins with mean slope gradients of 50%–59%, 60%–69% and >70%, respectively. This result contrast with that given by Robichaud et al. (2000) who recommend that LB should be installed on gradients of less than 40%; slopes with gradients greater than 75% should be particularly avoided. Therefore, and according to our results, LB and EB can be recommended as effective measures to reduce SC at any range of slope gradient. Considering the intrinsic differences of AIC_N between the T-A and UT-A and the observed changes of SC among the three scenarios ($\Delta\overline{AIC_N}_{(\text{T-A vs. UT-A})} = -1.96, -2.02$ and -2.52 in the Pre-Fire, Fire and Post-Fire scenarios), the actual contribution of the soil erosion barriers (LB + EB) to reduce SC in the whole T-A was of 26.6% of the total decrease of SC. The remaining 73.4% of the SC reduction in the T-A was explained by the vegetation recovery.

Regarding the spatial patterns of SC, clear changes appeared in the T-A, whereas no remarkable changes appeared in the UT-A (Fig. 4a). As a consequence, the histogram of the values of AIC_N in the T-A changed with a bimodal distribution more marked, showing a clear increase in the number of pixel with low SC (Fig. 4b). As the SfM-derived DEM was generated at very high spatial resolution, we can observe the spatial patterns of SC in detail. The soil erosion barriers not only modified the spatial pattern of overland flow, creating upslope flow lines parallel to the barrier until the flow reaches a discharge point, but also creating disconnected areas or small closed basins (Fig. 5a and b). Disconnectivity concerns features or processes that are too distant from each other in space or time, so that a change in one component or process does not influence another (Wohl et al., 2019). In our case, disconnectivity is associated with local topographic thresholds (lower elevation) –created by the barriers– that overland flow cannot exceed to found connectivity. At catchment scale, sediment disconnectivity has been evaluated in geomorphic studies and reservoir/lake siltation (e.g. Fryirs et al., 2007; Yang et al., 2019). However, in fire-affected forests, sediment disconnectivity is not a common topic. In a burnt drainage basin, Wester et al. (2014) identified structural and functional sediment disconnectivity in rill-gully threads due to the presence of dry ravel deposits and discontinuous sediment transport along the landscape compartments. To our knowledge, this is the first study that evaluates sediment disconnectivity at hillslope in a fire-affected forest after PFMP. In the UT-A, the effect of the remaining burnt trees and gullies was observed in detail, appearing flow lines that surround the trunks (Fig. 5c) and concentrated flow lines in the gully (Fig. 5d).

The average specific effectiveness of the log barriers (LB) and Easy-Barriers® (EB) in the whole T-A to reduce SC was of 11.3% and 13.4%, respectively (Table 5). These percentages become relevant if we take into account that the surface area affected by the LB and EB was only of 2.8% and 1.3%. Considering the total number of barriers, LB and EB reduced SC by 0.1%/LB and 0.3%/EB, respectively. These results should be interpreted with caution, as we computed structural SC and not functional SC –in order to calculate the specific effect of the barriers avoiding the 'noise' produced by the rainfall factor on the AIC computation process–. It is known that the actual effect of soil erosion barriers in fire-affected forest depends, among other factors, on the rainfall amount and intensity (high effectiveness for small rain events, and almost no treatment effect for rain events with larger return periods), and degradation over time of the barriers (Robichaud et al., 2008). Therefore, further research should be focused on the factors (e.g. soil depth, antecedent soil moisture, soil water storage capacity, overland flow velocity) and parameters (e.g. soil organic matter content, lifespan of barriers, human pressure –grazing, presence of running-mountain trails–, litter layer thickness) that could explain the observed high variability of the effectiveness of the different soil erosion control measures applied in fire-affected areas. For instance, Prats et al. (2012) found in Portugal that mulching proved highly effective at the eucalypt site, reducing the runoff coefficient 1.7 times and sediment losses 7.3
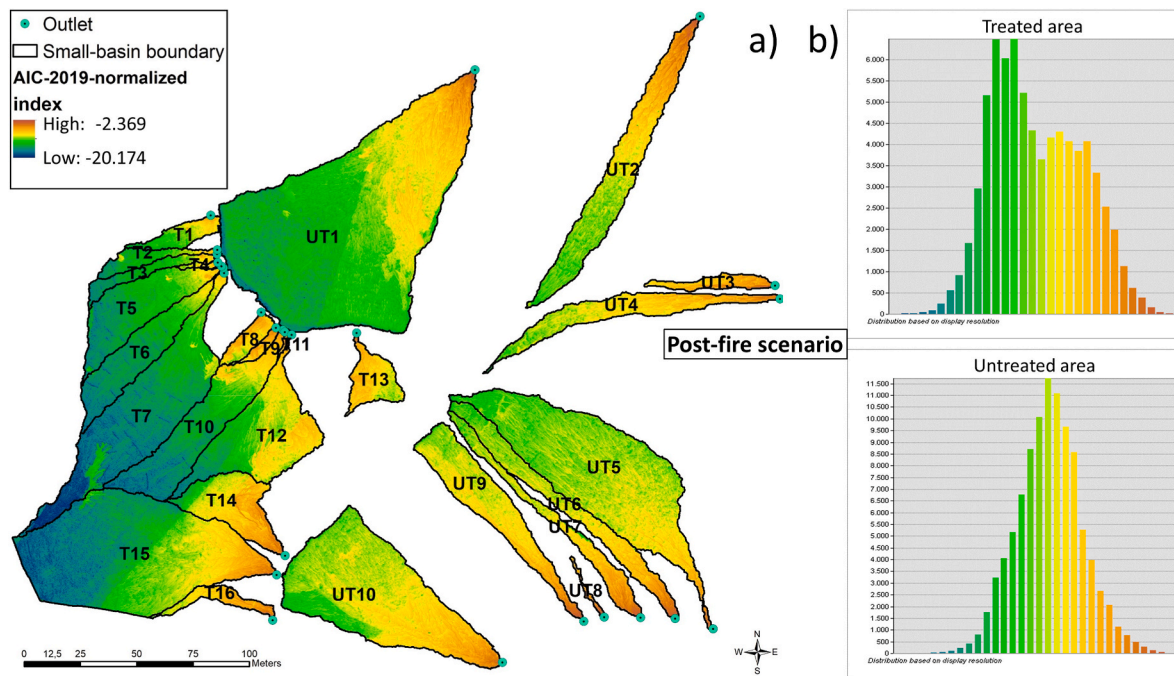
Fig. 4. Map of sediment connectivity (AIC$_N$) in the Post-fire scenario, and frequency distribution of the estimated values in the treated and untreated small basins.

times; whereas at the pine site, by contrast, mulching had no obvious effect. In ungauged areas, monitoring of sediment transport is almost impossible, and thus, numerical approaches like AIC become fundamental help tools.

3.3. Independent metrics

The convergence index (CI) was 15% lower in the T-A ($\overline{CI} = -0.53\%$ $\pm$ 20.37%) than in the UT-A ($\overline{CI} = -0.46\% \pm 15.47\%$), indicating a higher presence of sinks or concave surfaces in the T-A and higher presence of convex surfaces in the UT-A (Fig. 6a). This topographic characteristic was confirmed by the larger surface occupied by the flat areas (FA) in the T-A (ΣFA $= 66.2$ m^2) than in the UT-A (ΣFA $= 47.2$ m^2) (Fig. 6b). These results became more relevant after considering the total area of the different small basins, obtaining a ratio of 45.2 and 24.2 m^2 FA/ha in the T-A and UT-A, respectively. The higher density of flat areas in the T-A (1.9 times the density in the UT-A) can be associated with the presence of disconnected areas owing to the soil erosion barriers, agreeing with the results of lower SC estimated in the T-A at small basin and hillslope scales.

The mean values of flow width (FW) was 0.29% lower in the T-A ($\overline{FW} = 0.086$ m $\pm$ 0.027 m) than in the UT-A ($\overline{FW} = 0.085$ m $\pm$ 0.020 m). That means that wider flow channels are more frequent in the T-A –indicating less incisive flow– and narrower flow channels appear more frequently in the UT-A, which is characteristic of concentrated and erosive flow (Fig. 6c). Marked differences appeared in the LS-factor between the T-A ($\overline{LS} = 4.26 \pm 3.56$) and the UT-A ($\overline{LS} = 5.89 \pm 4.62$) indicating higher potential soil erosion in the small basins without PFMP (Fig. 6d). The computation of these metrics highlights the usefulness of drone imagery to characterise ground parameters in detail, especially in mountainous areas where terrain is complex (Sun and Zhang, 2018). Up-to-date and spatially accurate land information is critical to obtain trustworthy values and maps for future management (e.g., Ayele et al., 2018).

3.4. Implications for better PFMP

Conservation and restoration of degraded areas depend on various

socioeconomic factors that include ecosystem services (Petrakis et al., 2020). Post-fire management practices (PFMP) include different measures, some of them that provide benefits (e.g. log barriers, afforestation) whilst others can favour concentrated runoff and higher soil erosion, such as skid trails and burnt tree removal using heavy machinery (Martínez-Murillo et al., 2016, Martínez-Murillo et al., 2016). In order to minimize the duration of the so called "window of disturbance" (period between the fire and the total recovery of the ecosystems functions), PFMP have to be implemented in the first year after the fire (Sass et al., 2012). On one hand, the use of numerical approaches, such as the AIC, appears as a promising tool to evaluate in advance –and with limited computational-time demand– the effect of different PFMP on overland flow pathways and sediment connectivity. Therefore, we recommend the use of AIC by forest restoration companies and public administration for testing a number of restoration scenarios before starting field works. On the other hand, the usefulness of log barriers and Easy-Barriers® have been proved to reduce SC. However, we could not evaluate the impact of the new skid trail on the magnitude of SC due to the area covered by the drone imagery. In order to better estimate the overall effects of all PFMP, in terms of a balance between the damages and benefits, the skid trail should be included in a further study that will cover a larger area where the small basins including the skid trail could be evaluated. Skid trail effects remain on soil erosion several years after the fire, resulting in significantly elevated soil-erosion yields compared to soil conservation measures (Zituni et al., 2019). Therefore, further drone flights capturing the evolution of ground changes at very fine spatial resolution will offer the opportunity of quantifying the changes on soil loss and sediment transport pathways.

4. Conclusions

Drone imagery allowed generating a digital elevation model (DEM) of the fire-affected area at very fine spatial resolution capturing information of geomorphic and erosion features (e.g. slope gradient, residual topography, drainage area, convergence index, flow width, flat area and LS factor), as well as estimating the vegetation recovery –at the vegetation patch and shrub scales– 23 months after the fire. The new output-normalization approach of the aggregated index of connectivity (AIC)
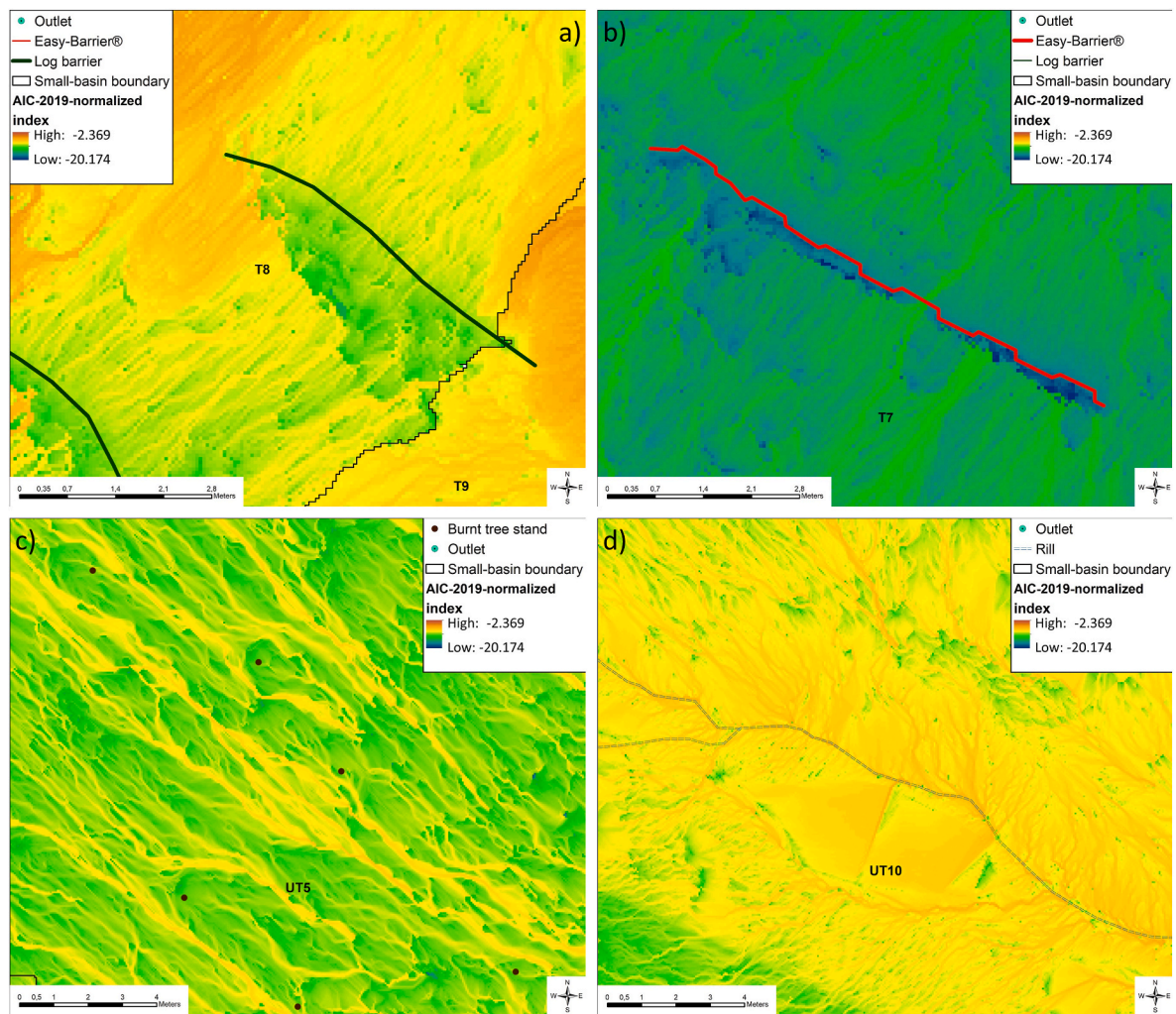
Fig. 5. Detail of the map of estimated sediment connectivity in the Post-fire scenario in the treated and untreated areas: (a) log barrier, (b) Easy-barrier®, (c) surrounding the burnt trees, and (d) in the gully.

Table 5
Estimated sediment connectivity (AIC_N) in the Post-fire scenario surrounding the log barriers (LB) and Easy-Barriers® (EB) in each small basin.

Zone	Basin	Log barriers			Easy-Barriers®		
Type	ID	mean	Rel. Value[a] (%)	Rel. Weight[b] (%)	mean	Rel. Value[a] (%)	Rel. Weight[b] (%)
Treated	T-1	−13.2	−19.9%	3.0%	−12.5	−13.4%	1.1%
	T-2	−15.2	−14.6%	6.9%	−13.2	+0.1%	0.9%
	T-3	−15.5	−15.2%	3.6%	−15.3	−14.3%	3.5%
	T-4	−7.8	+17.6%	1.9%	ND	ND	ND
	T-5	−15.7	−13.0%	5.0%	−14.4	−4.0%	1.6%
	T-6	−15.3	−5.4%	6.5%	−15.3	−5.4%	2.5%
	T-7	−16.0	−2.8%	4.3%	−16.0	−2.6%	2.3%
	T-8	−10.0	−23.0%	6.6%	−9.0	−10.4%	2.3%
	T-9	−9.7	−33.1%	2.0%	−7.4	−1.2%	2.7%
	T-10	−13.5	+2.5%	2.3%	−15.9	−15.5%	1.7%
	T-11	−6.6	+8.0%	8.6%	−8.6	−19.1%	6.1%
	T-12	−11.4	−2.3%	1.6%	−12.4	−11.3%	1.3%
	T-13	−8.9	−3.6%	1.6%	ND	ND	ND
	T-14	−9.4	−5.9%	1.0%	ND	ND	ND
	T-15	−15.1	−11.4%	0.6%	−15.9	−16.7%	0.1%
	T-16	−7.5	+3.9%	1.0%	ND	ND	ND
	All	*−14.5*	*−11.3%*	*2.8%*	*−14.8*	*−13.4%*	*1.3%*

[a] Estimated as the difference between $\overline{AIC_N}$ in the LB and $\overline{AIC_N}$ in the whole basin.
[b] Estimated as the weight of the AIC_N surrounding the barrier (sum of all pixels) and the values of AIC_N in the whole basin (sum of all pixels). ND: No data.
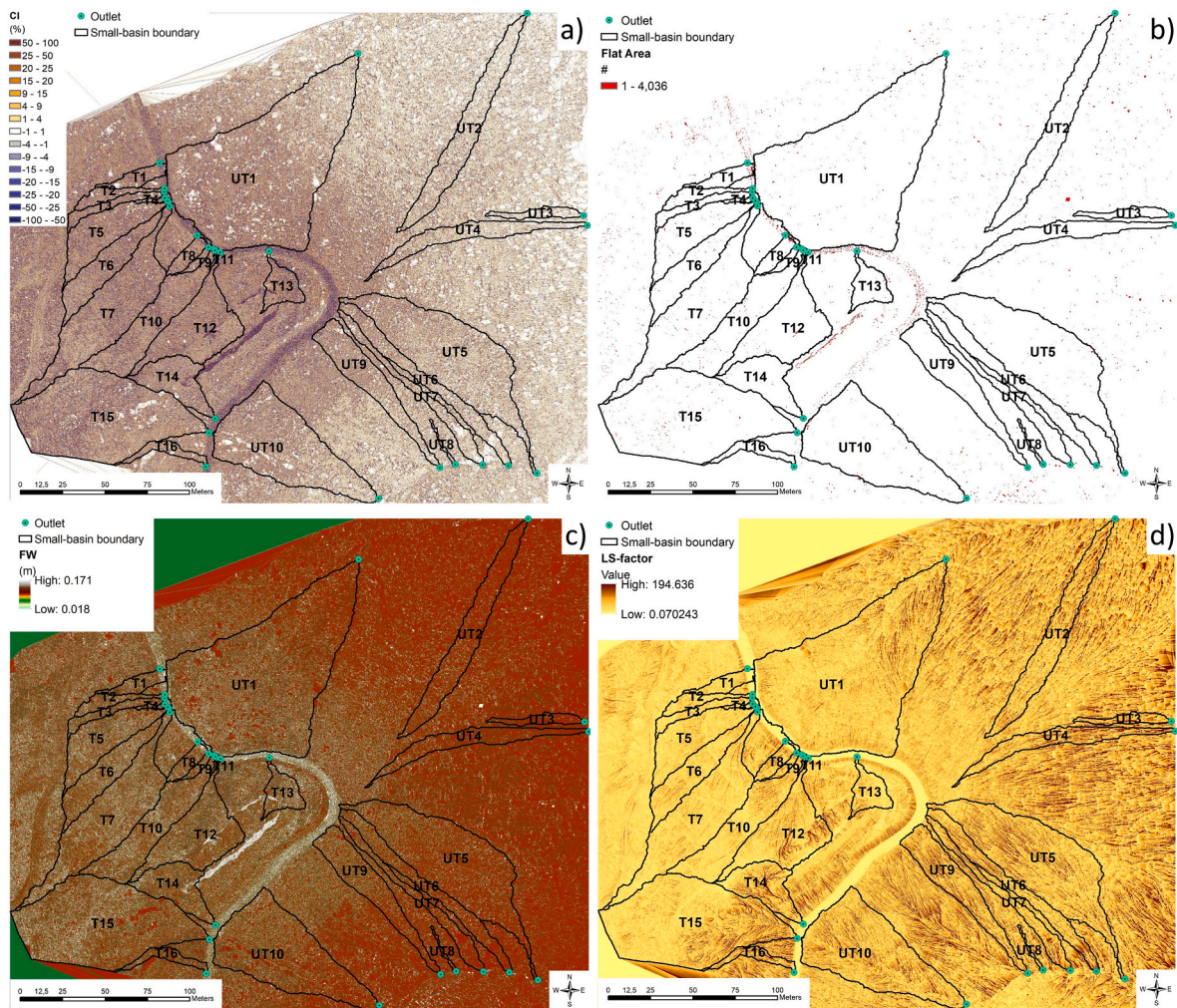
Fig. 6. Maps of the independent metrics: (a) convergence index (CI), (b) flat areas (FA), (c) flow width (FW) and (d) LS-RUSLE factor.

enabled comparing the calculated values and patterns of sediment connectivity (SC) in the different small basins of the treated (T-A) and untreated (UT-A) areas before and just after the fire and when all post-fire management practices were implemented –including the emerging vegetation recovery– obtaining clear changes among the areas and scenarios. Considering the intrinsic differences of SC between the T-A and UT-A and the evolution of SC among the three scenarios, the actual contribution of the soil erosion barriers to reduce SC in the whole T-A was 26.6% of the total decrease of SC. The remaining 73.4% of the SC reduction in the T-A was explained by the vegetation recovery. The overall reduction of SC in the T-A was 1.6 times the decrease of SC estimated in the UT-A. In particular, the average specific effectiveness of the log barriers (LB) and Easy-Barriers® (EB) to reduce SC was 11.3% and 13.4%, respectively. These percentages become relevant if we take into account that the surface area affected by the LB and EB is only 2.8% and 1.3%. The spatial pattern of overland flow was modified by the barriers appearing disconnected areas in some sections of the EB whilst disconnected areas in the UT-A are very scarce. The effectiveness of both types of barriers remains regardless the slope gradient, and thus, they can be seen as recommended measures to reduce SC in steep landscapes affected by forest fires. The independent metrics calculated with the DEM described features of higher soil erosion intensity in the UT-A supporting the results obtained with the AIC. Finally, we recommend the use of AIC by forest restoration companies and public administration as a practical tool to evaluate in advance –and with limited computational-time demand– a number of restoration scenarios before

starting field works.

Credit author statement

Manuel López-Vicente and Saskia Keesstra conceived of the present study, developed the theory and wrote the manuscript. Manuel López-Vicente and Henk Kramer performed the computations. All authors verified the analytical methods, supervised the findings of this work, discussed the results and contributed to the final manuscript.

Declaration of competing interest

The authors declare that they have no known competing financial interests or personal relationships that could have appeared to influence the work reported in this paper.

Environmental Research with Dr. Saskia Keesstra. We thank Mr. Agustín Bermejo Fernández, from the company 'Agroforestal Monte Vivo S.L.', for giving us access to the research area, information about the wildfire event and technical information and pictures of the 'Easy-Barriers' used in the study area.

Appendix A. Supplementary data

Supplementary data to this article can be found online at https://doi.org/10.1016/j.jenvman.2020.111510.

References

Albert-Belda, E., Bermejo-Fernández, A., Cerdà, A., Taguas, E.V., 2019. The use of Easy-Barriers to control soil and water losses in fire-affected land in Quesada, Andalusia, Spain. Sci. Total Environ. 690, 480–491. https://doi.org/10.1016/j.scitotenv.2019.06.303.

Anders, N., Valente, J., Masselink, R., Keesstra, S., 2019. Comparing filtering techniques for removing vegetation from UAV-based photogrammetric point clouds. Drones 3 (3), 61. https://doi.org/10.3390/drones3030061.

Anders, N., Smith, M., Suomalainen, J., Cammeraat, E., Valente, J., Keesstra, S., 2020. Impact of flight altitude and cover orientation on Digital Surface Model (DSM) accuracy for flood damage assessment in Murcia (Spain) using a fixed-wing UAV. Earth Sci. India. https://doi.org/10.1007/s12145-019-00427-7.

Aristeidis, K., Vasiliki, K., 2015. Evaluation of the post-fire erosion and flood control works in the area of Cassandra (Chalkidiki, North Greece). J. For. Res. 26 (1), 209–217. https://doi.org/10.1007/s11676-018-0741-3.

Ayele, G.T., Tebeje, A.K., Demissie, S.S., Belete, M.A., Jemberrie, M.A., Teshome, W.M., Mengistu, D.T., Teshale, E.Z., 2018. Time series land cover mapping and change detection analysis using geographic information system and remote sensing, Northern Ethiopia. Air Soil. Water Res. 11, 1–18. https://doi.org/10.1177/1178622117751603.

Badía, D., Martí, C., Aguirre, J., Echeverría, M.T., Ibarra, P., 2008. Erodibility and hydrology of arid burned soils: soil type and revegetation effects. Arid Land Res. Manag. 22 (4), 286–295. https://doi.org/10.1080/15324980802388231.

Badía, D., Sánchez, C., Aznar, J.M., Martí, C., 2015. Post-fire hillslope log debris dams for runoff and erosion mitigation in the semiarid Ebro Basin. Geoderma 237, 298–307. https://doi.org/10.1016/j.geoderma.2014.09.004.

Blake, W.H., Theocharopoulos, S.P., Skoulikidis, N., Clark, P., Tountas, P., Hartley, R., Amaxidis, Y., 2010. Wildfire impacts on hillslope sediment and phosphorus yields. J. Soils Sediments 10, 671–682. https://doi.org/10.1007/s11368-010-0201-y.

Borselli, L., Cassi, P., Torri, D., 2008. Prolegomena to sediment and flow connectivity in the landscape: a GIS and field numerical assessment. Catena 75 (3), 268–277. https://doi.org/10.1016/j.catena.2008.07.006.

Brogan, D.J., Nelson, P.A., MacDonald, L.H., 2019. Spatial and temporal patterns of sediment storage and erosion following a wildfire and extreme flood. Earth Surface Dynamics 7 (2), 563–590. https://doi.org/10.5194/esurf-7-563-2019.

Cerdà, A., 1998. Post-fire dynamics of erosional processes under Mediterranean climatic conditions. Zeitschrift fur Geomorphol 42, 373–398.

Cerdà, A., Lucas-Borja, M.E., Úbeda, X., Martínez-Murillo, J.F., Keesstra, S., 2017. *Pinus halepensis* M. versus *Quercus ilex* subsp. *Rotundifolia* L. runoff and soil erosion at pedon scale under natural rainfall in Eastern Spain three decades after a forest fire. For. Ecol. Manag. 400, 447–456. https://doi.org/10.1016/j.foreco.2017.06.038.

Chasmer, L.E., Hopkinson, C.D., Petrone, R.M., Sitar, M., 2017. Using multitemporal and multispectral airborne lidar to assess depth of peat loss and correspondence with a new active normalized burn ratio for wildfires. Geophys. Res. Lett. 44 (23), 11,851–11,859. https://doi.org/10.1002/2017GL075488.

De Koff, J.P., Graham, R.C., Hubbert, K.R., Wohlgemuth, P.M., 2006. Prefire and postfire erosion of soil nutrients within a chaparral watershed. Soil Sci. 171 (12), 915–928. https://doi.org/10.1097/01.ss.0000235231.02063.c2.

De Luis, M., González-Hidalgo, J.C., Raventós, J., 2003. Effects of fire and torrential rainfall on erosion in a Mediterranean gorse community. Land Degrad. Dev. 14 (2), 203–213. https://doi.org/10.1002/ldr.547.

Efthimiou, N., Psomiadis, E., Panagos, P., 2020. Fire severity and soil erosion susceptibility mapping using multi-temporal Earth Observation data: the case of Mati fatal wildfire in Eastern Attica, Greece. Catena 187. https://doi.org/10.1016/j.catena.2019.104320. Article number 104320.

Ellett, N.G., Pierce, J.L., Glenn, N.F., 2019. Partitioned by process: measuring post-fire debris-flow and rill erosion with Structure from Motion photogrammetry. Earth Surf. Process. Landforms 44 (15), 3128–3146. https://doi.org/10.1002/esp.4728.

EuropaPress, 2018. Newspaper article: 'La zona afectada por el incendio de Segura de la Sierra "se recupera bastante bien" un año después' in 20minutos. Free available in. https://www.20minutos.es/noticia/3413110/0/zona-afectada-por-incendio-segura-sierra-se-recupera-bastante-bien-ano-despues/(visited on. (Accessed 27 March 2020).

Fernández, C., Vega, J.A., Jiménez, E., Fonturbel, T., 2011. Effectiveness of three post-fire treatments at reducing soil erosion in Galicia (NW Spain). Int. J. Wildland Fire 20 (1), 104–114. https://doi.org/10.1071/WF09010.

Fox, D.M., Maselli, F., Carrega, P., 2008. Using SPOT images and field sampling to map burn severity and vegetation factors affecting post forest fire erosion risk. Catena 75 (3), 326–335. https://doi.org/10.1016/j.catena.2008.08.001.

Fryirs, K.A., Brierley, G.J., Preston, N.J., Kasai, M., 2007. Buffers, barriers and blankets: the (dis)connectivity of catchment-scale sediment cascades. Catena 70 (1), 49–67. https://doi.org/10.1016/j.catena.2006.07.007.

Gogorcena, Y., Sánchez-Monfort, M., López-Vicente, M., 2019. Grapevine yield and wine quality in ancient Spanish Pyrenean vineyards: influence of climatic and physiographic parameters. Vitis - Journal of Grapevine Research 58 (Special Issue), 103–110. https://doi.org/10.5073/vitis.2019.58.special-issue.103-110.

Gómez-Sánchez, E., Lucas-Borja, M.E., Plaza-Álvarez, P.A., González-Romero, J., Sagra, J., Moya, D., De Las Heras, J., 2019. Effects of post-fire hillslope stabilisation techniques on chemical, physicochemical and microbiological soil properties in Mediterranean forest ecosystems. J. Environ. Manag. 246, 229–238. https://doi.org/10.1016/j.jenvman.2019.05.150.

González, P., 2018. Newspaper article: 'Un año desde que las llamas cubrieron Segura de la Sierra' in DiarioJAÉN, 06 August 2018. Free available in. https://www.diariojaen.es/al-dia/un-ano-desde-que-las-llamas-cubrieron-segura-de-la-sierra-MD4445781 (visited on 27 March 2020).

González-Romero, J., Lucas-Borja, M.E., Plaza-Álvarez, P.A., Sagra, J., Moya, D., De Las Heras, J., 2019. Short-term effects of postfire check-dam construction on ephemeral stream vegetation in a semiarid climate of SE Spain. Sci. Total Environ. 671, 776–785. https://doi.org/10.1016/j.scitotenv.2019.03.366.

Gruber, S., Peckham, S., 2008. Land-surface parameters and objects in hydrology. In: Hengl, T., Reuter, H.I. (Eds.), Geomorphometry: Concepts, Software, Applications. Developments in Soil Science, vol. 33. Elsevier, pp. 293–308. Postprint available at: http://www.zora.uzh.ch.

Guo, Y., Senthilnath, J., Wu, W., Zhang, X., Zeng, Z., Huang, H., 2019. Radiometric calibration for multispectral camera of different imaging conditions mounted on a UAV platform. Sustainability 11 (4). https://doi.org/10.3390/su11040978 article 978.

Hooke, J., 2003. Coarse sediment connectivity in river channel systems: a conceptual framework and methodology. Geomorphology 56 (1–2), 79–94. https://doi.org/10.1016/S0169-555X(03)00047-3.

Hua, L., Shao, G., 2017. The progress of operational forest fire monitoring with infrared remote sensing. J. For. Res. 28 (2), 215–229. https://doi.org/10.1007/s11676-016-0361-8.

Igarashi, Y., Onda, Y., Wakiyama, Y., Konoplev, A., Zheleznyak, M., Lisovyi, H., Laptev, G., Damiyanovich, V., Samoilov, D., Nanba, K., Kirieiev, S., 2020. Impact of wildfire on ^{137}Cs and ^{90}Sr wash-off in heavily contaminated forests in the Chernobyl exclusion zone. Environ. Pollut. 259 https://doi.org/10.1016/j.envpol.2019.113764. Article number 113764.

Inbar, A., Lado, M., Sternberg, M., Tenau, H., Ben-Hur, M., 2014. Forest fire effects on soil chemical and physicochemical properties, infiltration, runoff, and erosion in a semiarid Mediterranean region. Geoderma 221–222, 131–138. https://doi.org/10.1016/j.geoderma.2014.01.015.

Inbar, M., Tamir, M., Wittenberg, L., 1998. Runoff and erosion processes after a forest fire in Mount Carmel, a Mediterranean area. Geomorphology 24 (1), 17–33. https://doi.org/10.1016/S0169-555X(97)00098-6.

Keeley, J.E., 2009. Fire intensity, fire severity and burn severity: a brief review and suggested usage. Int. J. Wildland Fire 18 (1), 116–126. https://doi.org/10.1071/WF07049.

Köthe, R., Gehrt, E., Böhner, J., 1996. Automatische Reliefanalyse für geowissenschaftliche Anwendun-gen – derzeitiger Stand und Weiterentwicklungen des Programms SARA. Arbeitshefte Geol. 1, 31–37.

Larsen, I.J., MacDonald, L.H., 2007. Predicting postfire sediment yields at the hillslope scale: testing RUSLE and Disturbed WEPP. Water Resour. Res. 43, W11412. https://doi.org/10.1029/2006WR005560.

Lee, C.W., Seo, J.I., Youn, H.J., Kim, K., 2014. Effectiveness of rehabilitation treatments on a slowly revegetating hillslope in a recently burned coastal forest, Republic of Korea. Landsc. Ecol. Eng. 10 (1), 249–260. https://doi.org/10.1007/s11355-013-0218-7.

López-Vicente, M., Álvarez, S., 2018. Influence of DEM resolution on modelling hydrological connectivity in a complex agricultural catchment with woody crops. Earth Surf. Process. Landforms 43 (7), 1403–1415. https://doi.org/10.1002/esp.4321.

López-Vicente, M., Ben-Salem, N., 2019. Computing structural and functional flow and sediment connectivity with a new aggregated index: a case study in a large Mediterranean catchment. Sci. Total Environ. 651 (1), 179–191. https://doi.org/10.1016/j.scitotenv.2018.09.170.

López-Vicente, M., González-Romero, J., Lucas-Borja, M.E., 2020. Forest fire effects on sediment connectivity in headwater sub catchments: evaluation of indices performance. Sci. Total Environ. 732 https://doi.org/10.1016/j.scitotenv.2020.139206 article 139206.

López-Vicente, M., Navas, A., Machín, J., 2009. Effect of physiographic conditions on the spatial variation of seasonal topsoil moisture in Mediterranean soils. Aust. J. Soil Res. 47 (5), 498–507. https://doi.org/10.1071/SR08250.

Lucas-Borja, M.E., Zema, D.A., Carrà, B.G., Cerdà, A., Plaza-Alvarez, P.A., Cózar, J.S., Gonzalez-Romero, J., Moya, D., de las Heras, J., 2018. Short-term changes in infiltration between straw mulched and non-mulched soils after wildfire in Mediterranean forest ecosystems. Ecol. Eng. 122, 27–31. https://doi.org/10.1016/j.ecoleng.2018.07.018.

Martin, Y.E., Johnson, E.A., Gallaway, J.M., Chaikina, O., 2011. Negligible soil erosion in a burned mountain watershed, Canadian Rockies: field and modelling investigations considering the role of duff. Earth Surf. Process. Landforms 36 (15), 2097–2113. https://doi.org/10.1002/esp.2236.

Martínez-Murillo, J.F., Hueso-González, P., Ruiz-Sinoga, J.D., Lavee, H., 2016. Short-term experimental fire effects in soil and water losses in southern of Spain. Land Degrad. Dev. 27 (5), 1513–1522. https://doi.org/10.1002/ldr.2504.

Martínez-Murillo, J.F., López-Vicente, M., 2018. Effect of salvage logging and check dams on simulated hydrological connectivity in a burned area. Land Degrad. Dev. 29 (3), 701–712. https://doi.org/10.1002/ldr.2735.

Martínez-Murillo, J.F., Neris, J., Hyde, K., Keizer, J.J., 2016. Advances towards an integrated assessment of fire effects on soils, vegetation and geomorphological processes. Land Degrad. Dev. 27 (5), 1314–1318. https://doi.org/10.1002/ldr.2520.

Mataix-Solera, J., Cerdà, A., Arcenegui, V., Jordán, A., Zavala, L.M., 2011. Fire effects on soil aggregation: a review. Earth Sci. Rev. 109 (1–2), 44–60. https://doi.org/10.1016/j.earscirev.2011.08.002.

Merino, A., Doni, S., Evelpidou, N., Ferreira, T., García-Arias, A.I., Masciandaro, G., Rodríguez-González, P.M., 2019. Best Practices in Evaluation and Restoration of Degraded Mediterranean Environments. Monografías do Ibader - Serie Territorio. Ibader. Universidade de Santiago de Compostela. Lugo. http://www.ibader.gal/ficha/547/924/Best-Practices-in-Evaluation-and-Restoration-of-Degraded-Mediterranean-Environments-2019-.html.

Post-fire management and restoration of southern European forests: managing forest ecosystems. In: Moreira, F., Arianoutsou, M., Corona, P., De las Heras, J. (Eds.), Managing Forest Ecosystems 24, 332. https://doi.org/10.1007/978-94-007-2208-8. Springer. ISBN 978-94-007-2207-1.

Nasta, P., Palladino, M., Ursino, N., Saracino, A., Sommella, A., Romano, N., 2017. Assessing long-term impact of land-use change on hydrological ecosystem functions in a Mediterranean upland agro-forestry catchment. Sci. Total Environ. 605–606, 1070–1082. https://doi.org/10.1016/j.scitotenv.2017.06.008.

Nishigaki, T., Sugihara, S., Kilasara, M., Funakawa, S., 2017. Surface runoff generation and soil loss under different soil and rainfall properties in the uluguru mountains, Tanzania. Land Degrad. Dev. 28 (1), 283–293. https://doi.org/10.1002/ldr.2499.

Nouwakpo, S.K., Williams, C.J., Pierson, F.B., Weltz, M.A., Kormos, P.R., Arslan, A., Al-Hamdan, O.Z., 2020. Effectiveness of prescribed fire to re-establish sagebrush steppe vegetation and ecohydrologic function on woodland-encroached sagebrush rangelands, Great Basin, USA: Part II: runoff and sediment transport at the patch scale. Catena 185. https://doi.org/10.1016/j.catena.2019.104301. Article number 104301.

Nunes, J.P., Naranjo-Quintanilla, P., Santos, J.M., Serpa, D., Carvalho-Santos, C., Rocha, J., Keizer, J.J., Keesstra, S.D., 2018. Afforestation, subsequent forest fires and provision of hydrological services: a model-based analysis for a mediterranean mountainous catchment. Land Degrad. Dev. 29 (3), 776–788. https://doi.org/10.1002/ldr.2776.

Panagos, P., Borrelli, P., Meusburger, K., Alewell, C., Lugato, E., Montanarella, L., 2015. Estimating the soil erosion cover-management factor at the European scale. Land Use Pol. 48, 38–50. https://doi.org/10.1016/j.landusepol.2015.05.021.

Pena, S.B., Abreu, M.M., Magalhães, M.R., Cortez, N., 2020. Water erosion aspects of land degradation neutrality to landscape planning tools at national scale. Geoderma 363. https://doi.org/10.1016/j.geoderma.2019.114093 article 114093.

Petrakis, R.E., Norman, L.M., Lysaght, O., Sherrouse, B.C., Semmens, D., Bagstad, K.J., Pritzlaff, R., 2020. Mapping perceived social values to support a respondent-defined restoration economy: case study in southeastern Arizona, USA. Air Soil. Water Res. 13, 1–16. https://doi.org/10.1177/1178622120913318.

Prats, S.A., Malvar, M.C., Coelho, C.O.A., Wagenbrenner, J.W., 2019. Hydrologic and erosion responses to compaction and added surface cover in post-fire logged areas: isolating splash, interrill and rill erosion. J. Hydrol. 575, 408–419. https://doi.org/10.1016/j.jhydrol.2019.05.038.

Prats, S.A., MacDonald, L.H., Monteiro, M., Ferreira, A.J.D., Coelho, C.O.A., Keizer, J.J., 2012. Effectiveness of forest residue mulching in reducing post-fire runoff and erosion in a pine and a eucalypt plantation in north-central Portugal. Geoderma 191, 115–124. https://doi.org/10.1016/j.geoderma.2012.02.009.

Raftoyannis, Y., Spanos, I., 2005. Evaluation of log and branch barriers as post-fire rehabilitation treatments in a Mediterranean pine forest in Greece. Int. J. Wildland Fire 14 (2), 183–188. https://doi.org/10.1071/WF04031.

Renard, K.G., Foster, G.R., Weesies, G.A., McCool, D.K., Yoder, D.C., 1997. Predicting Soil Erosion by Water: a Guide to Conservation Planning with the Revised Universal Soil Loss Equation (RUSLE). In: Handbook #703. US Department of Agriculture, Washington.

Robichaud, P.R., Beyers, J.L., Neary, D.G., 2000. Evaluating the Effectiveness of Postfire Rehabilitation Treatments. General Technical Report RMRS-GTR-63. U.S. Department of Agriculture, Forest Service, Rocky Mountain Research Station, Fort Collins, p. 85. https://www.fs.fed.us/rm/pubs/rmrs_gtr063.pdf. (Accessed 27 August 2020).

Robichaud, P.R., Lewis, S.A., Wagenbrenner, J.W., Brown, R.E., Pierson, F.B., 2020. Quantifying long-term post-fire sediment delivery and erosion mitigation effectiveness. Earth Surf. Process. Landforms 45 (3), 771–782. https://doi.org/10.1002/esp.4755.

Robichaud, P.R., Wagenbrenner, J.W., Brown, R.E., Wohlgemuth, P.M., Beyers, J.L., 2008. Evaluating the effectiveness of contour-felled log erosion barriers as a post-fire runoff and erosion mitigation treatment in the western United States. Int. J. Wildland Fire 17 (2), 255–273. https://doi.org/10.1071/WF07032.

Sass, O., Heel, M., Leistner, I., Stöger, F., Wetzel, K.F., Friedmann, A., 2012. Disturbance, geomorphic processes and recovery of wildfire slopes in North Tyrol. Earth Surf. Process. Landforms 37 (8), 883–894. https://doi.org/10.1002/esp.3221.

Shakesby, R.A., 2011. Post-wildfire soil erosion in the Mediterranean: review and future research directions. Earth Sci. Rev. 105 (3–4), 71–100. https://doi.org/10.1016/j.earscirev.2011.01.001.

Shin, P., Sankey, T., Moore, M.M., Thode, A.E., 2018. Evaluating unmanned aerial vehicle images for estimating forest canopy fuels in a ponderosa pine stand. Rem. Sens. 10 (8) https://doi.org/10.3390/rs10081266. Article number 1266.

Spanos, I., Raftoyannis, Y., Platis, P., Xanthopoulou, E., 2010. Post-fire management and recovery of a pine forest in Greece. Web Ecol. 10 (1), 27–31. https://doi.org/10.5194/we-10-27-2010.

Sun, Z., Zhang, Y., 2018. Using drones and 3D modeling to survey Tibetan architectural heritage: a case study with the multi-door stupa. Sustainability 10 (7). https://doi.org/10.3390/su10072259 article 2259.

Tang, H., McGuire, L.A., Rengers, F.K., Kean, J.W., Staley, D.M., Smith, J.B., 2019. Evolution of debris-flow initiation mechanisms and sediment sources during a sequence of postwildfire rainstorms. J. Geophys. Res.: Earth Surface 124 (6), 1572–1595. https://doi.org/10.1029/2018JF004837.

Tarolli, P., Cavalli, M., Masin, R., 2019. High-resolution morphologic characterization of conservation agriculture. Catena 172, 846–856. https://doi.org/10.1016/j.catena.2018.08.026.

USDA, 2008. Draft Science Documentation: Revised Universal Soil Loss Equation Version 2 (RUSLE2). United States Department of Agriculture (USDA), Agricultural Research Service, Washington, D.C. http://www.ars.usda.gov/Research/docs.htm?docid=6028.

Valenca, R., Ramnath, K., Dittrich, T.M., Taylor, R.E., Mohanty, S.K., 2020. Microbial quality of surface water and subsurface soil after wildfire. Water Res. 175 https://doi.org/10.1016/j.watres.2020.115672 article number 115672.

Van Eck, C.M., Nunes, J.P., Vieira, D.C.S., Keesstra, S., Keizer, J.J., 2016. Physically-based modelling of the post-fire runoff response of a forest catchment in Central Portugal: using field versus remote sensing based estimates of vegetation recovery. Land Degrad. Dev. 27 (5), 1535–1544. https://doi.org/10.1002/ldr.2507.

Velasco, L., 2018. Newspaper article: '«Brotes verdes» en El Yelmo un año después del gran incendio' in IDEAL, 03 August 2018. Free available in. https://www.ideal.es/jaen/provincia-jaen/brotes-verdes-yelmo-20180803212614-ntvo.html?ref=https%3F%2Fwww.google.es%2F (visited on. (Accessed 27 March 2020).

Vieira, D.C.S., Prats, S.A., Nunes, J.P., Shakesby, R.A., Coelho, C.O.A., Keizer, J.J., 2014. Modelling runoff and erosion, and their mitigation, in burned Portuguese forest using the revised Morgan-Morgan-Finney model. For. Ecol. Manag. 314, 150–165. https://doi.org/10.1016/j.foreco.2013.12.006.

Wester, T., Wasklewicz, T., Staley, D., 2014. Functional and structural connectivity within a recently burned drainage basin. Geomorphology 206, 362–373. https://doi.org/10.1016/j.geomorph.2013.10.011.

Wohl, E., Brierley, G., Cadol, D., Coulthard, T.J., Covino, T., Fryirs, K.A., Grant, G., Hilton, R.G., Lane, S.N., Magilligan, F.J., Meitzen, K.M., Passalacqua, P., Poeppl, R.E., Rathburn, S.L., Sklar, L.S., 2019. Connectivity as an emergent property of geomorphic systems. Earth Surf. Process. Landforms 44 (1), 4–26. https://doi.org/10.1002/esp.4434.

Wohlgemuth, P.M., Hubbert, K.R., Robichaud, P.R., 2001. The effects of log erosion barriers on post-fire hydrologic response and sediment yield in small forested watersheds, southern California. Hydrol. Process. 15 (15), 3053–3066. https://doi.org/10.1002/hyp.391.

Yair, A., Raz-Yassif, N., 2004. Hydrological processes in a small arid catchment: scale effects of rainfall and slope length. Geomorphology 61 (1–2), 155–169. https://doi.org/10.1016/j.geomorph.2003.12.003.

Yang, X., Lu, X., Ran, L., Tarolli, P., 2019. Geomorphometric assessment of the impacts of dam construction on river disconnectivity and flow regulation in the Yangtze basin. Sustainability 11 (12). https://doi.org/10.3390/su11123427 article 3427.

Yochum, S.E., Norman, J.B., 2015. Wildfire-induced flooding and erosion-potential modeling: examples from Colorado, 2012 and 2013. In: Proceedings of the 3rd Joint Federal Interagency Conference on Sedimentation and Hydrologic Modeling. April 19-23, 2015, Reno, Nevada, USA.

Zavala, L.M., González, F.A., Jordán, A., 2009. Fire-induced soil water repellency under different vegetation types along the Atlantic dune coast-line in SW Spain. Catena 79 (2), 153–162. https://doi.org/10.1016/j.catena.2009.07.002.

Zhang, J., Zhou, L., Ma, R., Jia, Y., Yang, F., Zhou, H., Cao, X., 2019. Influence of soil moisture content and soil and water conservation measures on time to runoff initiation under different rainfall intensities. Catena 182. https://doi.org/10.1016/j.catena.2019.104172. Article number 104172.

Zituni, R., Wittenberg, L., Malkinson, D., 2019. The effects of post-fire forest management on soil erosion rates 3 and 4 years after a wildfire, demonstrated on the 2010 Mount Carmel fire. Int. J. Wildland Fire 28 (5), 377–385. https://doi.org/10.1071/WF18116.